Model predictive control of an automotive waste heat recovery system

Model predictive control of an automotive waste heat recovery system

H. Koppauer[a,*], W. Kemmetmüller[a], A. Kugi[a]

[a] *Automation and Control Institute, TU Wien, Gußhausstraße 27/29, 1040 Vienna, Austria*

Abstract

This paper proposes a model predictive control strategy for an Organic Rankine Cycle based waste heat recovery system. The control strategy uses a prediction model based on gain scheduling of local models, which results in a quadratic program to efficiently calculate the optimal control inputs. To ensure an optimal system operation, the reference values are obtained from a steady-state optimization. To capture a model-plant mismatch, the control concept features an EKF-based estimator of the model uncertainties. Simulations on a validated simulation model show that this control strategy can track the optimal reference very well, even for a large model-plant mismatch.

Keywords: Waste heat recovery, Organic Rankine Cycle, Nonlinear control, Model predictive control, Automotive systems

1. Introduction

Research on fuel efficient technologies for internal combustion engines has become very important in the last years to reduce the fuel costs and to meet the strict regulations on CO_2 emissions. Concerning this matter, heavy-duty trucks offer a high fuel saving potential because they have a high fuel consumption combined with a high yearly mileage.

A state-of-the-art heavy-duty diesel engine can reach fuel efficiencies of 45% in best operating points, while approximately one third of the fuel energy is lost through the exhaust gas. Thus, current research focuses on systems that recover waste heat from the exhaust gas, to improve the overall system efficiency, see, e.g., [1]. Among the investigated concepts, waste heat recovery (WHR) systems based on the Organic Rankine Cycle (ORC) are a promising technology for heavy-duty applications, cf. [2, 3, 4]. The expected fuel savings range from 5% to 10%, see, e.g., [5].

Fig. 1 depicts an ORC WHR system with one evaporator, where the hot exhaust gas evaporates an organic working fluid at a high pressure level. The vaporized working fluid expands over an expansion machine to a lower pressure level and its internal energy converts into mechanical energy, which can be directly used for traction [6] or stored in an energy storage system [5]. The hot working fluid then condenses in the condenser and the residual heat is transferred to the cooling water, see, e.g., [5, 6].

In the past, research on ORC WHR systems was primarily concerned with the cycle topology (number and arrangement of the evaporators) and the suitability of certain working fluids, see, e.g., [7, 8, 9, 10]. In this context, a former work of the authors focused on calculating optimal steady-state operating points with the corresponding control inputs for given exhaust gas mass flows and inlet temperatures, cf. [11]. The dynamic operation of automotive ORC systems brings along additional demands on the control design because the exhaust gas heat flow rates are changing in a highly dynamic way and several state constraints have to be met to ensure a safe system operation, see, e.g., [12, 13]. A suitable control strategy must avoid dryout and temperature shocks of the evaporators, cf. [4], as well as the decomposition of the working fluid. Moreover, the control algorithm has to account for the considerable nonlinearities of the ORC system, mainly of the heat exchangers, to yield a high control and system performance. These challenges make the control of the high-pressure part of the ORC WHR system an interesting field of research.

The ORC systems examined in the literature differ in their system topologies (e.g., the number of evaporators [10]), the type of expansion machine (e.g., turbine [6], screw [8] or scroll expander [14]), and the number and the type of the actuators. The common control goal is to control the system states at the evaporator outlet or at the inlet of the expansion machine. In recent years, a number of different control concepts have been presented in the literature. In [3], the authors propose a combination of a model-based nonlinear feedforward controller including a parameter adaption with a PID feedback controller. A similar concept is presented in [15], but instead of a single PID controller a gain scheduled PID controller is used to account for the system nonlinearities. Moreover, in [16] a nonlinear feedforward controller is combined with a gain scheduling of LQR controllers and corresponding Luenberger observers. To consider a model-plant mismatch, the heat transfer parameters of the feedforward model are adapted online and the linear models for the Luenberger observers are extended with an unknown output disturbance. The authors of [4] use a Linear Quadratic Integral (LQI) controller to control an ORC system with multiple control inputs. Compared to a pair of single PID controllers,

*Corresponding author.
Email addresses: koppauer@acin.tuwien.ac.at (H. Koppauer), kemmetmueller@acin.tuwien.ac.at (W. Kemmetmüller), kugi@acin.tuwien.ac.at (A. Kugi)

Post-print version of the article: H. Koppauer, W. Kemmetmüller, and A. Kugi, "Model predictive control of an automotive waste heat recovery system", *Control Engineering Practice*, vol. 81, pp. 28–42, 2018. doi: 10.1016/j.conengprac.2018.09.005

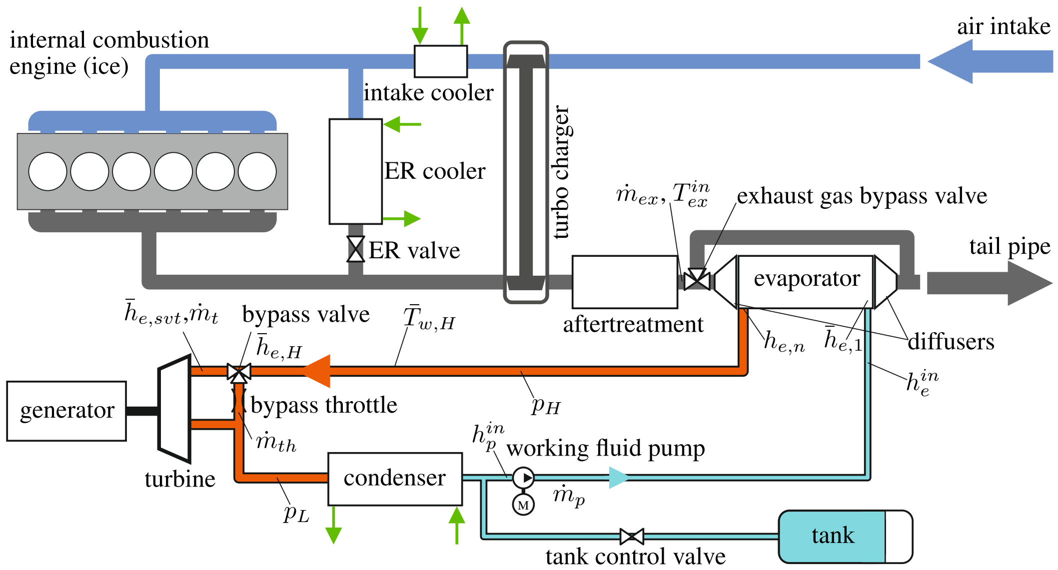

Figure 1: Sketch of the considered WHR system with one evaporator.

the LQI controller shows a superior control performance.

The control schemes presented so far do not allow to consider state constraints in a systematic way. Several other works, e.g., [13, 17, 18], examined the application of model predictive control (MPC) to automotive ORC systems. MPC takes into account the state and the actuator constraints as well as the measured disturbances and can handle multi-input multi-output control problems, cf. [19, 20]. To allow for a real-time implementation on an automotive electronic control unit (ECU), a linear MPC based on three reduced order system models is presented in [13], which considers the system nonlinearities by switching the prediction models depending on the actual exhaust gas heat flow rate. This switching may cause bumps of the estimated states and consequently larger control deviations after changing the prediction model. To avoid this, the rate of change of the control inputs has to be restricted for this control concept. Further investigations show that using a nonlinear MPC could improve the control performance (time with superheated vapor at the evaporator outlet) by $\approx$ 10%, but it is not feasible for a real-time implementation, cf. [13]. Nonlinear MPC using a simplified model is also investigated in simulations in [17]. To account for the system nonlinearities, the authors of [18] propose an adaptive linear MPC for the evaporating temperature, which uses a system model of two first order transfer functions plus time delay with gain and time constants depending on the actual superheating of the working fluid and the exhaust gas mass flow. Both quantities were identified for several operating points and fitted with two-dimensional polynomials. This method considers only one actuating variable and no coupling between the output variables.

Analyzing the results of these articles concerning MPC indicates that the system control performance can be improved by systematically taking into account the system nonlinearities. However, a nonlinear MPC is not real-time capable for an automotive ECU. Thus, this article presents an MPC concept that approximately considers the system nonlinearities, but only requires a similar computational effort as linear MPC. As mentioned in [16], an appropriate control strategy for an ORC WHR system must be able to cope with an unavoidable model-plant mismatch. Therefore, a suitable method is investigated to identify the model-plant mismatch and consider it in the MPC model.

In general, an ORC system with two evaporators in parallel offers a high recovering potential, but brings along higher requirements on the control strategies, see, e.g., [10, 11]. Hence, as a first step for designing an appropriate MPC strategy for dual evaporator WHR systems, this article focuses on controlling the working fluid state at the turbine inlet of an ORC WHR system with one evaporator, as it is presented in Fig. 1.

This article is organized as follows: First, Section 2 describes the system under investigation and its specific properties. Next, the mathematical system model and its gain scheduling approximation is given in Section 3. Section 4 explains the developed control scheme in detail. Finally, Section 5 discusses the simulation results for the presented control scheme.

2. System description

Fig. 1 shows the considered test-bench setup of the WHR system. An Euro VI six cylinder diesel engine, coupled to an electrical brake, discharges hot exhaust gas with highly varying mass flows and temperatures. The pump delivers the working fluid (ethanol) to a counterflow evaporator, which is placed in the exhaust gas path after the exhaust aftertreatment. There, the exhaust heat is used to heat up and evaporate the working fluid. If the system restrictions do not allow any further heat transfer to the working fluid, the proportional exhaust gas bypass valve can reduce the exhaust gas mass flow through the evaporator. Possible system restrictions are, e.g., the maximum temperature

Post-print version of the article: H. Koppauer, W. Kemmetmüller, and A. Kugi, “Model predictive control of an automotive waste heat recovery system”, *Control Engineering Practice*, vol. 81, pp. 28–42, 2018. DOI: 10.1016/j.conengprac.2018.09.005

of the working fluid or the maximum pressure due to the system construction.

A radial turbine is utilized to convert the internal energy of the vaporized working fluid into mechanical power. It also drives the generator, which is operated to yield an optimal rotational speed of the turbine, cf. [5, 13]. To prevent droplet erosion, a minimum vapor quality has to be ensured at the turbine inlet. If the vapor quality is too low or no turbine power is required, the bypass switching valve is actuated and the working fluid expands over the bypass throttle. After the expansion, the superheated or two-phase fluid condenses in the condenser. The tank control valve allows to connect the low-pressure part of the WHR system to the working fluid tank, but it is closed during normal operation. Several components, which are necessary for safety reasons, are not displayed in Fig. 1, since they are not relevant for the subsequent controller design.

3. Mathematical Model

This section summarizes the control-oriented mathematical system model for describing the dynamics of the high-pressure part of the WHR system and analyzes the impact of the model-plant mismatch. Based on these results, a suitable approximation of the dynamical model is proposed that is based on a gain scheduling of local system models.

3.1. Control-oriented model

In [11], a detailed model of the considered WHR system is given and investigated in a parallel dual evaporator setup. It is shown that this model is able to accurately reproduce the dynamic system behavior measured on a test-bench in the entire operating range. This section gives a control-oriented mathematical model of the high-pressure part of the considered single evaporator system that is based on the validated model given in [11]. For a detailed derivation of the given equations, the reader is referred to [11].

The original model according to [11] of the single evaporator high-pressure part features a high accuracy, but also a high complexity with 65 states. Thus, this model is not directly suitable for a model based controller design, as e.g., model predictive control. To reduce the model complexity, several effects are neglected that have only small influence on the system dynamics: (i) The increase of enthalpy from the pump inlet to the pump outlet is small and thus neglected. This entails that the specific evaporator inlet enthalpy h_e^{in} is equal to the specific enthalpy h_p^{in} at the inlet of the working fluid pump. (ii) The short piping from the bypass switching valve to the turbine is neglected and consequently the turbine mass flow $\dot{m}_t$ is calculated using the states at the inlet of the bypass switching valve. This is feasible because the enthalpy loss from the bypass switching valve inlet to the turbine inlet has only little influence on the turbine mass flow. (iii) Investigations showed that the dynamics of the exhaust gas temperature along the evaporator is significantly faster than the temperature dynamics of the working fluid and the separating wall. Thus, a quasi-stationary approach is used for the exhaust gas temperature, see, also, [3, 21].

The dynamics of the evaporator is described by the conservation of mass and energy. For this, it is assumed that the multi-channel plate evaporator can be described by an equivalent model with one effective channel for the working fluid, one for the exhaust gas, and the separating wall. For the mathematical model equal pressure is assumed in the entire high-pressure part and thus the working fluid pressure in the evaporator is equal to the turbine inlet pressure p_H. Furthermore, constant density ρ_w and isobaric heat capacities c_w, $c_{p,ex}$ of the wall and the exhaust gas are presumed. To derive a finite-dimensional model, the computational region is discretized along the spatial coordinate z into $i = 1, \ldots, n = 20$ finite volumes of length Δz and the finite-volume method is applied, see [11]. The resulting set of ordinary differential equations for the averaged specific enthalpy of the working fluid $\bar{h}_{e,i}$ and the averaged wall temperature $\bar{T}_{w,i}$ in each finite volume is given as, see [11] for more details,

$$\frac{\mathrm{d}\bar{h}_{e,i}}{\mathrm{d}t} = \frac{\frac{\dot{m}_{e,i-1}}{\Delta z}(h_{e,i-1} - h_{e,i}) - \partial A^c \bar{\alpha}_{e,i}(\bar{T}_{e,i} - \bar{T}_{w,i})}{A_e^c\left(\bar{\rho}_{e,i} + \dfrac{\partial \bar{\rho}_{e,i}}{\partial \bar{h}_{e,i}}(\bar{h}_{e,i} - h_{e,i})\right)} \tag{1a}$$

$$\frac{\mathrm{d}\bar{T}_{w,i}}{\mathrm{d}t} = \frac{\partial A^c \bar{\alpha}_{e,i}(\bar{T}_{e,i} - \bar{T}_{w,i}) + \partial A^c \alpha_{ex}(\bar{T}_{ex,i} - \bar{T}_{w,i})}{A_w^c c_w \rho_w}, \tag{1b}$$

with the specific enthalpies $h_{e,i-1}$, $h_{e,i}$ at the finite volume borders. The averaged exhaust gas temperature $\bar{T}_{ex,i} = (T_{ex,i-1} + T_{ex,i})/2$ results from

$$T_{ex,i-1} = \frac{2\dot{m}_{ex,ev} c_{p,ex} T_{ex,i} + \partial A^c \alpha_{ex} \Delta z (T_{ex,i} - 2\bar{T}_{w,i})}{2\dot{m}_{ex,ev} c_{p,ex} - \partial A^c \alpha_{ex} \Delta z}, \tag{2}$$

where $T_{ex,i-1}$ and $T_{ex,i}$ denote the exhaust gas temperatures at the finite volume borders. At the exhaust gas inlet, the temperature $T_{ex,n}$ is equal to the exhaust gas inlet temperature T_{ex}^{in}. The averaged density $\bar{\rho}_{e,i}$ and temperature $\bar{T}_{e,i}$ are calculated from the averaged specific enthalpy $\bar{h}_{e,i}$ and the turbine inlet pressure p_H using the constitutive equations for the working fluid from [11], which are a modified version of the working fluid model from [21]. Furthermore, the wall cross sectional area A_w^c, the channel cross sectional area A_e^c, and the heat exchanging boundary ∂A^c describe the evaporator geometry. The heat transfer coefficient α_{ex} from the exhaust gas to the wall is a function of the exhaust gas mass flow $\dot{m}_{ex}$. Moreover, the heat transfer coefficient $\bar{\alpha}_{e,i}$ from the working fluid to the wall depends on the working fluid inlet mass flow $\dot{m}_{e,0}$, on the turbine inlet pressure p_H, and on the vapor fraction $\gamma(h_e, p_H) = (h_e - h_e'(p_H))/(h_e''(p_H) - h_e'(p_H))$, with the saturation values $h_e'(p_H)$ of liquid and $h_e''(p_H)$ of vapor.

The working fluid mass flow $\dot{m}_{e,i}$ at the outlet of each finite volume reads as

$$\dot{m}_{e,i} = \dot{m}_{e,i-1} - \Delta z A_e^c \frac{\partial \bar{\rho}_{e,i}}{\partial \bar{h}_{e,i}} \frac{\mathrm{d}\bar{h}_{e,i}}{\mathrm{d}t}, \quad i = 1, \ldots, n, \tag{3}$$

with the finite-volume inlet mass flows $\dot{m}_{e,i-1}$. At the first finite volume, the mass flow $\dot{m}_{e,0}$ is equal to the mass flow $\dot{m}_p$

Post-print version of the article: H. Koppauer, W. Kemmetmüller, and A. Kugi, “Model predictive control of an automotive waste heat recovery system”, *Control Engineering Practice*, vol. 81, pp. 28–42, 2018. DOI: 10.1016/j.conengprac.2018.09.005
The content of this post-print version is identical to the published paper but without the publisher’s final layout or copy editing.

of the working fluid pump and $h_{e,0} = h_p^{in}$ holds. The exhaust gas mass flow through the evaporator is calculated as

$$\dot{m}_{ex,ev} = \chi_{ex}\dot{m}_{ex}, \tag{4}$$

with the position of the exhaust gas bypass valve $\chi_{ex} \in [0, 1]$ and the exhaust gas mass flow $\dot{m}_{ex}$ at the outlet of the exhaust aftertreatment.

The model for the average specific enthalpy $\bar{h}_{e,H}$ in the high-pressure part piping from the evaporator to the bypass switching valve and for the average piping wall temperature $\bar{T}_{w,H}$ reads as [11]

$$\begin{aligned} V_{e,H}\bar{\rho}_{e,H}\frac{\mathrm{d}\bar{h}_{e,H}}{\mathrm{d}t} =& \dot{m}_{e,n}\left(h_{e,n} - \bar{h}_{e,H}\right) \\ &- \alpha_{e,H}A^s_{e,H}\left(\bar{T}_{e,H} - \bar{T}_{w,H}\right), \end{aligned} \tag{5a}$$

$$\begin{aligned} V_{w,H}c_w\rho_w\frac{\mathrm{d}\bar{T}_{w,H}}{\mathrm{d}t} =& \alpha_{e,H}A^s_{e,H}\left(\bar{T}_{e,H} - \bar{T}_{w,H}\right) \\ &- \alpha_{a,H}A^s_{a,H}\left(\bar{T}_{w,H} - T_{amb}\right), \end{aligned} \tag{5b}$$

with the volume $V_{e,H}$ of the high-pressure part piping, the heat transfer coefficient $\alpha_{e,H}$ and the surface area $A^s_{e,H}$ from the working fluid to the wall, the wall volume $V_{w,H}$ (specific heat capacity c_w, density ρ_w), and the heat transfer coefficient $\alpha_{a,H}$ and the effective surface area $A^s_{a,H}$ to the ambiance (ambient temperature T_{amb}). Furthermore, the averaged density $\bar{\rho}_{e,H}$ and the averaged temperature $\bar{T}_{e,H}$ are calculated from the turbine inlet pressure p_H and the specific enthalpy $\bar{h}_{e,H}$.

As mentioned before, equal pressure p_H is assumed in the entire high-pressure part (evaporator and pipings). The mass balance for this part yields

$$\frac{\mathrm{d}p_H}{\mathrm{d}t} = \frac{\dot{m}_{e,n} - \dot{m}_{sv} - V_{e,H}\dfrac{\partial\bar{\rho}_{e,H}}{\partial\bar{h}_{e,H}}\dfrac{\mathrm{d}\bar{h}_{e,H}}{\mathrm{d}t}}{\xi + V_{e,H}\dfrac{\partial\bar{\rho}_{e,H}}{\partial p_H}} \tag{6}$$

with

$$\xi = A^c_e\sum_{i=1}^{n}\Delta z\left(\frac{\partial\bar{\rho}_{e,i}}{\partial p_H}\right), \tag{7}$$

which takes into account the influence of the compressible fluid in the evaporator. The mass flow $\dot{m}_{sv}$ into the bypass switching valve is equal to the turbine mass flow $\dot{m}_t$ or to the bypass throttle mass flow $\dot{m}_{th}$, depending on the operation in turbine mode or bypass mode. The turbine mass flow $\dot{m}_t$ and the bypass throttle mass flow $\dot{m}_{th}$ are given as a function of the turbine inlet pressure p_H, the turbine outlet pressure p_L, and the specific inlet enthalpy. As described before, the piping at the turbine inlet is neglected and $\bar{h}_{e,H}$ is used as inlet enthalpy for the calculation of both mass flows. For more details on the calculation of the mass flow, see [11].

Subsequently, this model is summarized as

$$\dot{\mathbf{x}} = \mathbf{f}^n(\mathbf{x}, \mathbf{u}, \mathbf{v}) \tag{8a}$$

$$\mathbf{y} = \mathbf{C}\mathbf{x} \tag{8b}$$

with the system states

$$\mathbf{x} = [\bar{h}_{e,1}, .., \bar{h}_{e,n}, \bar{T}_{w,1}, .., \bar{T}_{w,n}, p_H, \bar{h}_{e,H}, \bar{T}_{w,H}]^{\mathrm{T}}, \tag{9}$$

the control inputs

$$\mathbf{u} = [\dot{m}_p, \chi_{ex}]^{\mathrm{T}}, \tag{10}$$

the exogenous inputs

$$\mathbf{v} = [\dot{m}_{ex}, T^{in}_{ex}, h^{in}_p, T_{amb}, p_L]^{\mathrm{T}}, \tag{11}$$

and the measured outputs

$$\mathbf{y} = [h_{e,n}, p_H, \bar{h}_{e,H}]^{\mathrm{T}}. \tag{12}$$

This model has $2n + 3 = 43$ system states.

3.2. Influence of a model-plant mismatch

The model of Section 3.1 is capable of representing the system dynamics quite well, see [11]. Nevertheless, a model-plant mismatch is inevitable in the practical application due to the following reasons: (i) The model is based on a number of simplifications and approximated functions, e.g., for the heat transfer coefficients and the constitutive equations of the working fluid. (ii) Certain properties of the system (in particular the heat transfer coefficients) are subject to significant variations during operation, e.g., caused by fouling in the evaporator. (iii) The exogenous input $\mathbf{v}$ is not exactly known due to measurement errors in the practical application. In particular, the mass flow $\dot{m}_{ex}$ and the temperature T^{in}_{ex} of the exhaust gas at the evaporator inlet can be afflicted with a significant error, since $\dot{m}_{ex}$ is a calculated value of the ECU and sooting can influence the temperature measurement. Thus, a practically feasible control strategy must be robust or adapt to this model-plant mismatch. To study the influence of these effects, first the impact of the exogenous input variables $\dot{m}_{ex}$, T^{in}_{ex}, T_{amb}, and h^{in}_p on the model outputs $\bar{h}_{e,H}$ and p_H is analyzed. These two output quantities are relevant, since $\bar{h}_{e,H}$ represents the controlled variable and p_H is used for calculating the reference value of $\bar{h}_{e,H}$, see Section 4.1. For this analysis the relative sensitivity

$$\kappa_{y_i,v_j} = \frac{\Delta y_i/y_i}{\Delta v_j/v_j} \tag{13}$$

of the steady-state output changes Δy_i due to input variations Δv_j is calculated at optimal steady-state operating points covering the entire engine operating range. Fig. 2 depicts the resulting relative sensitivities at the optimal operating points sorted for the pressure p_H of the investigated operating points in ascending order. It can be seen that variations of the exhaust gas inputs $\dot{m}_{ex}$ and T^{in}_{ex} have the largest influence on the output variables. The influence of the ambient temperature T_{amb} increases for small pressures p_H and corresponding small working fluid heat flow rates $\dot{Q}_{e,n} = \dot{m}_p h_{e,n}$ at the evaporator outlet. However, this influence is, as the influence of h^{in}_p, small compared to the influence of $\dot{m}_{ex}$ and T^{in}_{ex}. Moreover, it can be expected that T_{amb} and h^{in}_p are known rather accurately in the real system. It has to be noted that the influence of the exogenous input p_L does not have to be considered in this study, since at optimal steady-state operating points p_L is below the critical pressure and thus does not have an influence on p_H and $\bar{h}_{e,H}$.

Post-print version of the article: H. Koppauer, W. Kemmetmüller, and A. Kugi, “Model predictive control of an automotive waste heat recovery system”, *Control Engineering Practice*, vol. 81, pp. 28–42, 2018. DOI: 10.1016/j.conengprac.2018.09.005

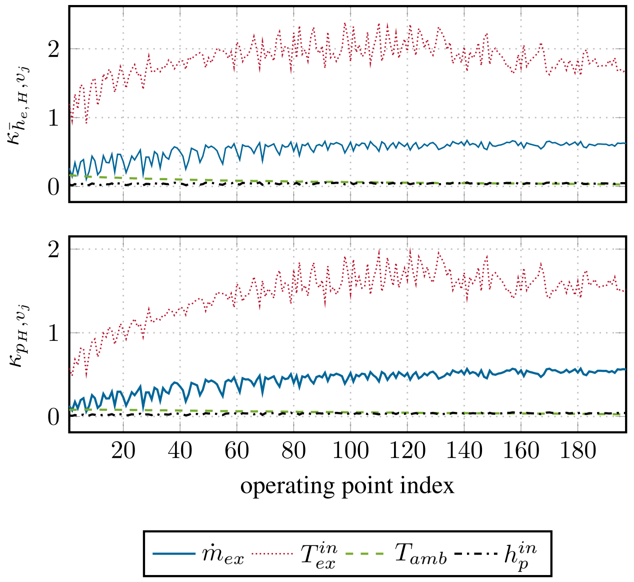

Figure 2: Relative sensitivity of the outputs $\bar{h}_{e,H}$ and p_H due to variations of the exogenous inputs $\dot{m}_{ex}$, T_{ex}^{in}, T_{amb}, and h_p^{in}.

As briefly mentioned before, the heat transfer coefficients are the model parameters that can exhibit the largest deviations from their nominal values. Moreover, the heat transfer coefficients α_{ex} from the exhaust gas to the wall and $\bar{\alpha}_{e,i}$ from the wall to the working fluid directly influence the heat transfer from the exhaust gas to the working fluid in the evaporator. The heat transfer coefficient α_{ex} on the exhaust gas side is significantly lower than the heat transfer coefficient on the working fluid side. Thus, it dominates the steady-state heat transfer determined by the local heat transmission coefficient $k_i = \alpha_{ex}\bar{\alpha}_{e,i}/(\alpha_{ex}+\bar{\alpha}_{e,i})$, cf. [3], and variations of α_{ex} have a significantly larger influence on the system behavior. The same holds true when analyzing the heat transfer at the high-pressure part piping. Here, the heat transfer coefficient $\alpha_{a,H}$ from the piping wall to the ambiance is small compared to $\alpha_{e,H}$.

This discussion shows that errors of the heat flow from the exhaust gas to the working fluid - either due to errors in $\dot{m}_{ex}$, T_{ex}^{in} or in α_{ex} - and from the working fluid to the ambiance ($\alpha_{a,H}$) can have a significant influence on the model accuracy. This can lead to a low performance of the model-based control strategy in the practical application.

To approximately consider this effect in the model for the controller design, the model equations (1b) and (5b) of the wall temperatures of the evaporator and the high-pressure part piping, respectively, are augmented in the form

$$
\begin{aligned}
A_w^c c_w \rho_w \frac{\mathrm{d}\bar{T}_{w,i}}{\mathrm{d}t} =& \partial A^c \bar{\alpha}_{e,i}\left(\bar{T}_{e,i} - \bar{T}_{w,i}\right) \\
&+ \partial A^c \alpha_{ex}\left(\bar{T}_{ex,i} - \bar{T}_{w,i}\right) + \frac{\mu_i}{\Delta z}\Delta\dot{Q}_{ex}
\end{aligned}
\tag{14a}
$$

$$
\begin{aligned}
V_{w,H} c_w \rho_w \frac{\mathrm{d}\bar{T}_{w,H}}{\mathrm{d}t} =& \alpha_{e,H} A_{e,H}^s\left(\bar{T}_{e,H} - \bar{T}_{w,H}\right) \\
&- \alpha_{a,H} A_{a,H}^s\left(\bar{T}_{w,H} - T_{amb}\right) + \Delta\dot{Q}_H .
\end{aligned}
\tag{14b}
$$

Here, the heat flow rates $\Delta\dot{Q}_{ex}$ and $\Delta\dot{Q}_H$ are introduced to account for the errors in the transferred heat due to the previously mentioned possible model-plant mismatches. In the subsequent controller design, the heat flow rates $\Delta\dot{Q}_{ex}$ and $\Delta\dot{Q}_H$ will be treated as unknown parameters, which have to be estimated by a suitable observer, see Section 4.4. The heat flow rates are introduced to capture the model errors due to an inaccurate knowledge of the heat flow between the exhaust gas and the evaporator wall and between the high-pressure part piping and the ambiance, which are the main sources of the model-plant mismatch. However, these two heat flow rates also approximately cover other model-plant mismatches, e.g., resulting from the simplified constitutive equations of the working fluid, cf. [11].

The shaping function μ_i is introduced in (14a) to approximately capture the spatial dependence of the influence of the model errors for the evaporator. Due to the nonlinearity of the evaporator model, the specific shape of μ_i strongly depends on the actual model errors (actual exhaust gas quantities, actual heat transfer coefficient α_{ex}). Hence, there is no clear indication for a suitable choice of μ_i. However, investigations for several model errors (combinations of parameter deviations of α_{ex} and measurement errors of the exhaust gas quantities) show that the model errors usually have the highest influence near the exhaust gas inlet at $i = n$. Thus, the performance of the state estimator (see Section 4.4) was tested in simulations with different model errors, and a linear and a quadratic shaping function μ_i. The simulation results showed a slightly better estimation of the evaporator states and a better closed-loop performance with a quadratic shaping function

$$
\mu_i = 1 + \left(\frac{i-1}{n-1}\right)^2,
\tag{15}
$$

which is thus used in this work.

3.3. Gain scheduling model

The reduced order mathematical model represents a set of numerically stiff nonlinear differential equations whose time integration requires a high computational effort. Thus, it is not well suited for a nonlinear MPC strategy, which is considered in this work, cf. [13, 22]. In this section, a gain scheduling model based on quasilinear local model approximations is proposed. These local system approximations are calculated at nominal operating points and combined using a scheduling variable, which characterizes the system behavior at the current

Post-print version of the article: H. Koppauer, W. Kemmetmüller, and A. Kugi, "Model predictive control of an automotive waste heat recovery system", *Control Engineering Practice*, vol. 81, pp. 28–42, 2018. DOI: 10.1016/j.conengprac.2018.09.005

operating point, cf. [23, 24]. As it will be shown later, the use of such a model reduces the computation of the optimal control inputs to solving a quadratic program (QP).

Given the discussion of the previous section, the model (8)-(12) with (14) can be written as

$$\dot{\mathbf{x}} = \mathbf{f}(\mathbf{x}, \mathbf{u}, \mathbf{v}, \boldsymbol{\theta}) \tag{16a}$$
$$\mathbf{y} = \mathbf{C}\mathbf{x} \tag{16b}$$

with the heat flow rates

$$\boldsymbol{\theta} = \left[\Delta\dot{Q}_{ex}, \Delta\dot{Q}_{H}\right]^{\mathrm{T}}. \tag{17}$$

In the nominal case, the vector $\boldsymbol{\theta}$ is equal to zero and $\mathbf{f}(\mathbf{x}, \mathbf{u}, \mathbf{v}, \boldsymbol{\theta}) = \mathbf{f}^n(\mathbf{x}, \mathbf{u}, \mathbf{v})$ from (8a).

To identify a suitable scheduling variable for the local linear model approximations, the behavior of the nonlinear model is evaluated around stationary optimal operating points. To do so, the exhaust gas mass flow $\dot{m}_{ex}$ and temperature T_{ex}^{in} at the inlet of the evaporator are measured at a test bench for n_{SOP} steady-state operating points, which cover the relevant operating range of the WHR system, see the blue circles (○) in Fig. 3. Furthermore, the ambient temperature T_{amb}, the turbine outlet pressure p_L, and the specific pump inlet enthalpy h_p^{in} are selected as the average of their typical value. For each of these values $\mathbf{v}_{s,l} = [\dot{m}_{ex,l}, T_{ex,l}^{in}, h_p^{in}, T_{amb}, p_L]$, $l = 1, \ldots, n_{SOP}$, optimal steady-state operating points are calculated for the nominal system model $\boldsymbol{\theta} = \mathbf{0}$ by solving

$$\mathbf{0} = \mathbf{f}(\mathbf{x}_{s,l}, \mathbf{u}_{s,l}, \mathbf{v}_{s,l}, \mathbf{0}) \tag{18a}$$
$$0 = \bar{h}_{e,H,s,l} - \bar{h}_{e,H}^{ref}(p_{H,s,l}), \tag{18b}$$

for $\mathbf{x}_{s,l}$ and $\mathbf{u}_{s,l}$. The optimal reference value $\bar{h}_{e,H}^{ref}(p_{H,s,l})$ for the specific enthalpy $\bar{h}_{e,H,s,l}$ was derived from the optimal steady-state system operating points and will be explained in more detail in Section 4.1. For the solution, $\chi_{ex,s,l} = 1$ is utilized, which implies that the entire exhaust gas mass flow passes through the evaporator.

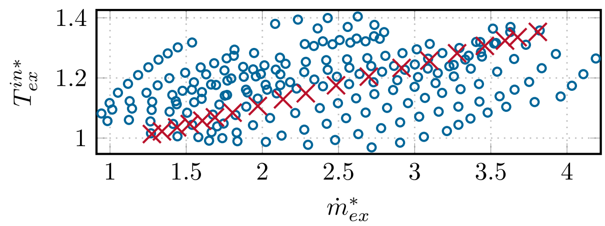

Figure 3: Normalized steady-state exhaust gas mass flows $\dot{m}_{ex}^*$ and inlet temperatures T_{ex}^{in*} of the evaporator.

Remark 1. *Note that all quantities indicated by the superscript $*$ are normalized quantities, obtained by relating the quantities to the reference values $\bar{h}_{e,H}^0$, $\bar{T}_{e,H}^0$, $\dot{m}_p^0$, p_H^0, and n_t^0 (reference rotational speed of the turbine) of a maximum power operating point. All powers (also the exhaust gas inlet heat flow rates $\dot{Q}_{ex}^{in} = c_{p,ex}\dot{m}_{ex}(T_{ex}^{in} - T_{amb})$) are related to the corresponding maximum shaft power P_t^0 of the turbine.*

In the next step, the local behavior of the nonlinear system around these optimal steady-state operating points is analyzed by performing small steps $\Delta\dot{m}_{p,l}$ of the pump mass flow $\dot{m}_p$ in the form $\Delta\dot{m}_{p,l} = 0.05\dot{m}_{p,s,l}$, with the pump mass flow $\dot{m}_{p,s,l}$ of the optimal steady-state operating point l. Fig. 4 shows the step response of the nonlinear system for 4 selected operating points with increasing exhaust gas inlet heat flow rate $\dot{Q}_{ex}^{in} = c_{p,ex}\dot{m}_{ex}(T_{ex}^{in} - T_{amb})$. Here, OP 1 corresponds to the smallest and OP 4 to the largest value. It can be clearly seen that the system dynamics becomes significantly faster for larger values of $\dot{Q}_{ex}^{in}$.

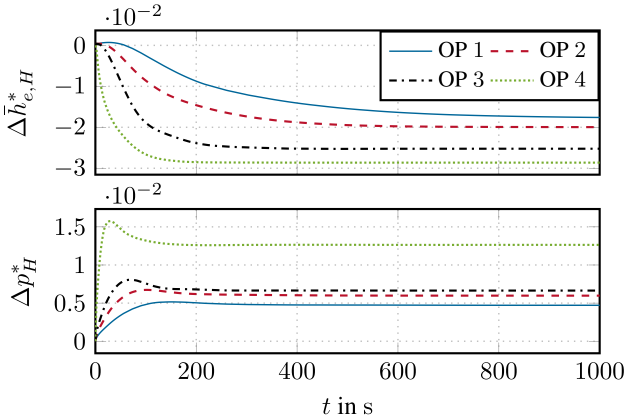

Figure 4: Normalized step response from the input $\Delta\dot{m}_p$ to the outputs $\Delta\bar{h}_{e,H}$ and Δp_H for selected optimal steady-state operating points.

In order to analyze this behavior for all chosen optimal operating points, Fig. 5 depicts the rise time τ from 0 % to 63 % of the final value and the stationary gain $G = \lim_{t\to\infty} \Delta\bar{h}_{e,H}(t)/\Delta\dot{m}_p$ of the step response from the input $\Delta\dot{m}_p$ to the output $\Delta\bar{h}_{e,H}$ as a function of $\dot{Q}_{ex}^{in}$. There is a strong correlation between $\dot{Q}_{ex}^{in}$ and these parameters of the step response, which indicates that $\dot{Q}_{ex}^{in}$ would be a meaningful scheduling variable.[1] This result is also reported in [13], where $\dot{Q}_{ex}^{in}$ is utilized as the switching variable in an MPC strategy for a double evaporator WHR system. In contrast, the authors of [16] utilize the exhaust gas mass flow $\dot{m}_{ex}$ as scheduling variable for LQR controllers. Both variables, however, have the drawback that they rely on quantities of the exhaust gas. In the real application, the exhaust gas mass flow is not measured, but only calculated based on models of the combustion engine in the ECU, which can yield rather large errors in $\dot{m}_{ex}$ and $\dot{Q}_{ex}^{in}$.

To circumvent this problem, the correlation between the optimal values of p_H and $\dot{Q}_{ex}^{in}$ is analyzed in more detail. Fig. 6 shows that there is an almost linear relation between these quantities, which suggests that p_H can be used as gain scheduling variable instead of $\dot{Q}_{ex}^{in}$. Utilizing p_H is beneficial in the real application, since this pressure is directly measured in the sys-

[1] The deviations from the general trend of the rise time τ and the gain G for small values of $\dot{Q}_{ex}^{in}$ are related to operating points with low exhaust gas inlet temperatures and a large superheating at the evaporator outlet, which is required to account for the considerable heat loss in the piping.

Post-print version of the article: H. Koppauer, W. Kemmetmüller, and A. Kugi, "Model predictive control of an automotive waste heat recovery system", *Control Engineering Practice*, vol. 81, pp. 28–42, 2018. DOI: 10.1016/j.conengprac.2018.09.005
The content of this post-print version is identical to the published paper but without the publisher's final layout or copy editing.

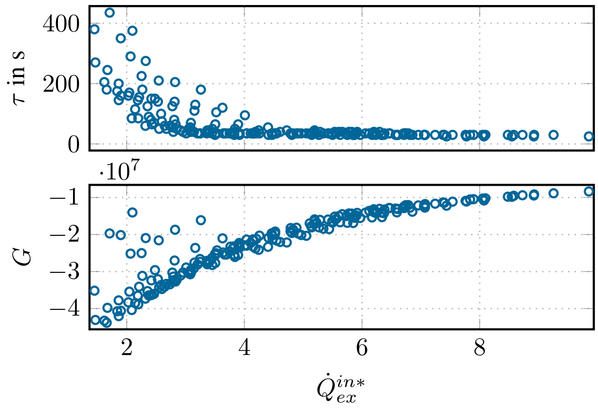

Figure 5: Time constant τ and stationary gain G of the step response from the input $\Delta \dot{m}_p$ to the output $\Delta \bar{h}_{e,H}$ as a function of the normalized exhaust gas inlet heat flow rate $\dot{Q}_{ex}^{in*}$.

tem and thus known rather accurately. Therefore, p_H is chosen as scheduling variable in this contribution.

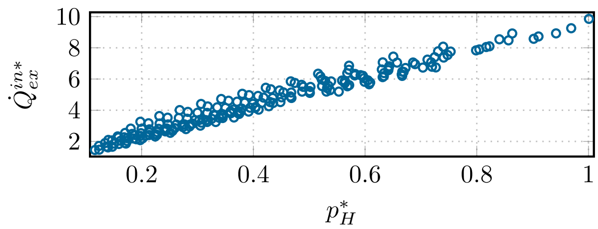

Figure 6: Relation of the normalized exhaust gas inlet heat flow rate $\dot{Q}_{ex}^{in*}$ and the normalized optimal steady-state pressure p_H^*.

Of course, it does not make sense to calculate a local linearized model for each of the stationary optimal operating points depicted in Fig. 3-6. Thus, a reduced set of optimal operating points has to be selected, which represents the overall operating range of the WHR system, cf. [25, 26]. For this, Fig. 3 is considered again. It was shown that the exhaust gas inlet heat flow rate $\dot{Q}_{ex}^{in}$ is a good indicator for the resulting system behavior. This quantity is basically proportional to the product of the exhaust gas mass flow $\dot{m}_{ex}$ and its temperature T_{ex}^{in}. Thus, it makes sense to choose a set of n_{OP} values of these two quantities that lie on a straight line, which ranges from the minimal to the maximum value of $\dot{Q}_{ex}^{in}$ typically occurring in the system. To account for the larger change in the system behavior for small values of $\dot{Q}_{ex}^{in}$, more points are used for low exhaust gas heat flow rates, see the red crosses (×) in Fig. 3.

With the selected set of n_{OP} nominal steady-state operating points $\mathbf{x}_{s,l}, \mathbf{u}_{s,l}, \mathbf{v}_{s,l}$, $l = 1, \ldots, n_{OP}$, the local system behavior can be approximated by the partially linearized models

$$
\begin{aligned}
\Delta\dot{\mathbf{x}}_l + \dot{\mathbf{x}}_{s,l} \cong& \mathbf{f}(\mathbf{x}_{s,l}, \mathbf{u}_{s,l}, \mathbf{v}, \boldsymbol{\theta}) + \left.\frac{\partial \mathbf{f}}{\partial \mathbf{x}}\right|_{\mathbf{x}_{s,l},\mathbf{u}_{s,l},\mathbf{v},\boldsymbol{\theta}} \Delta\mathbf{x}_l \\
&+ \left.\frac{\partial \mathbf{f}}{\partial \mathbf{u}}\right|_{\mathbf{x}_{s,l},\mathbf{u}_{s,l},\mathbf{v},\boldsymbol{\theta}} \Delta\mathbf{u}_l \qquad (19a)\\
\mathbf{y}_l =& \mathbf{C}(\mathbf{x}_{s,l} + \Delta\mathbf{x}_l), \qquad (19b)
\end{aligned}
$$

with $\Delta\mathbf{x}_l = \mathbf{x} - \mathbf{x}_{s,l}$ and $\Delta\mathbf{u}_l = \mathbf{u} - \mathbf{u}_{s,l}$, where the linearization is only performed with respect to $\mathbf{x}$ and $\mathbf{u}$. The nonlinear behavior of the system due to $\mathbf{v}$ is still reflected in these models in $\mathbf{f}(\mathbf{x}_{s,l}, \mathbf{u}_{s,l}, \mathbf{v}, \boldsymbol{\theta})$, which yields a significantly improved approximation accuracy compared to a full linearization. Examining $(\partial\mathbf{f}/\partial\mathbf{x})(\mathbf{x}_{s,l}, \mathbf{u}_{s,l}, \mathbf{v}, \boldsymbol{\theta})$ and $(\partial\mathbf{f}/\partial\mathbf{u})(\mathbf{x}_{s,l}, \mathbf{u}_{s,l}, \mathbf{v}, \boldsymbol{\theta})$ in detail shows that they can be rather well approximated by $\mathbf{A}_l = (\partial\mathbf{f}/\partial\mathbf{x})(\mathbf{x}_{s,l}, \mathbf{u}_{s,l}, \mathbf{v}_{s,l}, \mathbf{0})$ and $\mathbf{B}_l = (\partial\mathbf{f}/\partial\mathbf{u})(\mathbf{x}_{s,l}, \mathbf{u}_{s,l}, \mathbf{v}_{s,l}, \mathbf{0})$, respectively. Thus, the local partially linearized models can be written in the form

$$
\begin{aligned}
\Delta\dot{\mathbf{x}}_l =& \mathbf{A}_l\Delta\mathbf{x}_l + \mathbf{B}_l\Delta\mathbf{u}_l + \mathbf{f}(\mathbf{x}_{s,l}, \mathbf{u}_{s,l}, \mathbf{v}, \boldsymbol{\theta}) \qquad (20a)\\
\mathbf{y}_l =& \mathbf{C}(\mathbf{x}_{s,l} + \Delta\mathbf{x}_l). \qquad (20b)
\end{aligned}
$$

The corresponding discrete time models are obtained based on the assumptions $\mathbf{u}(t) = \mathbf{u}_k$, $\mathbf{v}(t) = \mathbf{v}_k$, and $\boldsymbol{\theta}(t) = \boldsymbol{\theta}_k$ for $k\tau_s \leq t < (k+1)\tau_s$, with the sampling time τ_s. They read as

$$
\begin{aligned}
\Delta\mathbf{x}_{k+1,l} =& \boldsymbol{\Phi}_l\Delta\mathbf{x}_{k,l} + \boldsymbol{\Gamma}_l\Delta\mathbf{u}_{k,l} + \mathbf{N}_{k,l} \qquad (21a)\\
\mathbf{y}_{k,l} =& \mathbf{C}(\mathbf{x}_{s,l} + \Delta\mathbf{x}_{k,l}) \qquad (21b)
\end{aligned}
$$

with $\boldsymbol{\Phi}_l = \exp(\mathbf{A}_l\tau_s)$, $\boldsymbol{\Gamma}_l = \int_0^{\tau_s}\exp(\mathbf{A}_l\tau)\mathrm{d}\tau\mathbf{B}_l$, and $\mathbf{N}_{k,l} = \int_0^{\tau_s}\exp(\mathbf{A}_l\tau)\mathrm{d}\tau\mathbf{f}(\mathbf{x}_{s,l}, \mathbf{u}_{s,l}, \mathbf{v}_k, \boldsymbol{\theta}_k)$.

To approximate the output of the nonlinear system in the entire operating range, the outputs of these n_{OP} local partially linearized models are combined as

$$
\mathbf{y}_k = \sum_{l=1}^{n_{OP}} \zeta_l(p_{H,k})\mathbf{y}_{k,l}, \qquad (22)
$$

with the validity functions $\zeta_l(p_{H,k})$, cf. [24]. The validity functions $\zeta_l(p_{H,k})$ are defined as

$$
\zeta_l(p_{H,k}) = \begin{cases} 0 & \text{for } p_{H,k} < p_{H,s,l-1} \\ \frac{p_{H,k} - p_{H,s,l-1}}{p_{H,s,l} - p_{H,s,l-1}} & \text{for } p_{H,s,l-1} \leq p_{H,k} < p_{H,s,l} \\ \frac{p_{H,s,l+1} - p_{H,k}}{p_{H,s,l+1} - p_{H,s,l}} & \text{for } p_{H,s,l} \leq p_{H,k} < p_{H,s,l+1} \\ 0 & \text{for } p_{H,k} \geq p_{H,s,l+1} \end{cases} \qquad (23)
$$

with the pressures $p_{H,s,l}$, $l = 1, \ldots, n_{OP}$, of the nominal operating points. The chosen validity functions (23) lead to a linear interpolation between the outputs of two partially linearized models (21).

To analyze the approximation quality of the output combination (22), the system behavior is discussed around an optimal steady-state operating point with the pressure $p_{H,o}$ (exhaust gas inputs $\dot{m}_{ex,o}$ and $T_{ex,o}^{in}$), which lies between the nominal operating points $p_{H,i}$ and $p_{H,i+1}$. To do so, the proposed output combination (22) is compared to the output of the nonlinear model (16) and the outputs of the local partially linearized

Post-print version of the article: H. Koppauer, W. Kemmetmüller, and A. Kugi, "Model predictive control of an automotive waste heat recovery system", *Control Engineering Practice*, vol. 81, pp. 28–42, 2018. DOI: 10.1016/j.conengprac.2018.09.005

models (21) at the nominal operating points i and $i+1$. This comparison considers a step in the working fluid mass flow $\dot{m}_p(t) = \dot{m}_{p,o}(1 + 0.05\sigma(t))$, with the mass flow $\dot{m}_{p,o}$ at the chosen operating point and the Heaviside function $\sigma(t)$.

Fig. 7 depicts the results of the system outputs $\bar{h}_{e,H}$ and p_H. As can be seen, the gain scheduling model (gs) approximates the dynamics of both output variables very well with only small steady-state errors with respect to the nonlinear model (nl). These stationary model errors are smaller than the model inaccuracies of the nonlinear model, which have to be considered in the controller design anyway. In comparison, the fixed local partially linearized models (pl i, pl $i+1$) show a significantly worse accuracy. Another benefit of the chosen output combination (22) compared to simply switching between local models (see, e.g., [13]) is that it results in a smooth transition between the local models.

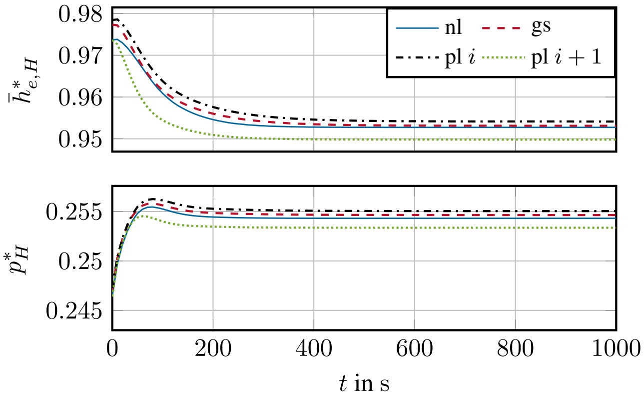

Figure 7: Comparison of the normalized step response from $\dot{m}_p$ to $\bar{h}_{e,H}$ and p_H of the nonlinear model (nl), the gain scheduling model (gs), and the local partially linearized models (pl i, pl $i+1$) - with $p_{H,i} \leq p_H \leq p_{H,i+1}$.

To demonstrate the advantage of using a partial linearization with respect to $\mathbf{x}$ and $\mathbf{u}$ for the output combination (22), this model is compared with a gain scheduling model using a full linearization with respect to the exogenous inputs $\mathbf{v}$ as well. Fig. 8 and 9 show the simulation results for operating points with low and medium engine load. While both models approximate the system dynamics of the nonlinear system rather well, the proposed partial linearization (20a) leads to significantly smaller steady-state deviations. This is because it considers the nonlinear system behavior due to the exhaust gas inputs $\dot{m}_{ex,o}$ and $T^{in}_{ex,o}$ in the term $\mathbf{f}(\mathbf{x}_{s,l}, \mathbf{u}_{s,l}, \mathbf{v}_o, \boldsymbol{\theta})$, $l = 1, \ldots, n_{OP}$, with $\mathbf{v}_o = [\dot{m}_{ex,o}, T^{in}_{ex,o}, h^{in}_p, T_{amb}, p_L]$, cf. (20a).

4. Control strategy

This section describes the proposed model predictive control strategy.

4.1. Control objective

The main control objective is to maximize the recovered energy. This can be equivalently formulated in the form that the optimal reference $\bar{h}^{ref}_{e,H}$ for the specific enthalpy $\bar{h}_{e,H}$ should be tracked. The optimal reference is derived from the results of the steady-state optimization in [11] and reads as

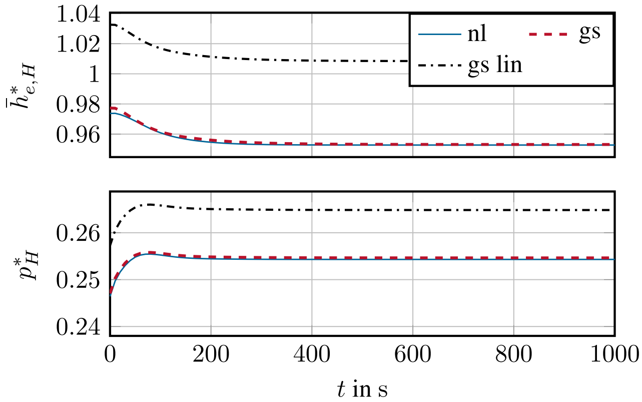

Figure 8: Comparison of the normalized step response from $\dot{m}_p$ to $\bar{h}_{e,H}$ and p_H of the nonlinear model (nl), the gain scheduling model (gs) and a gain scheduling model using linear models (gs lin) - medium engine load.

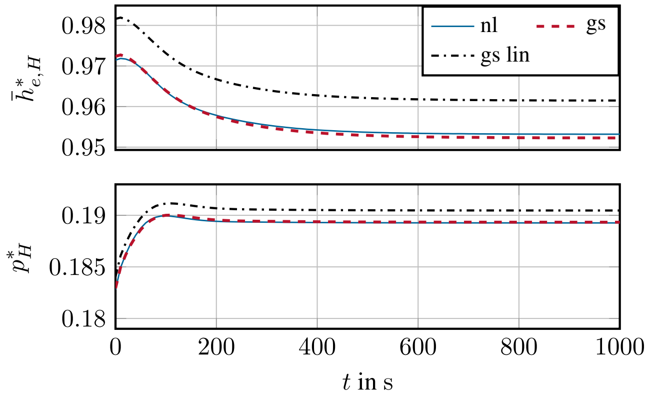

Figure 9: Comparison of the normalized step response from $\dot{m}_p$ to $\bar{h}_{e,H}$ and p_H of the nonlinear model (nl), the gain scheduling model (gs) and a gain scheduling model using linear models (gs lin) - low engine load.

$$\bar{h}^{ref}_{e,H}(p_H) = h''_e(p_H) + \Delta h^p_{sh}(p_H) \tag{24}$$

with the specific enthalpy $h''_e(p_H)$ of saturated vapor. This reference brings along that the superheating of the working fluid in the high-pressure part piping should be as low as possible with a pressure dependent safety gap $\Delta h^p_{sh}(p_H)$ to prevent the occurrence of two-phase fluid at the turbine inlet. The safety gap is introduced to account for the thermal losses in the piping from the bypass switching valve to the turbine inlet.

The thermal losses to the turbine inlet have a higher impact on the working fluid enthalpy for small working fluid heat flow rates, which are associated with low exhaust gas heat flow rates $\dot{Q}^{in}_{ex}$ and, equivalently, low values of the pressure p_H. To compensate for this effect, the safety gap $\Delta h^p_{sh}(p_H)$ in the reference is higher for small values of p_H (small values of the exhaust gas heat flow rates). For exhaust gas inlet temperatures T^{in}_{ex} below a minimal temperature $T^{in}_{ex,min}$, the required superheating Δh^p_{sh} cannot be reached. This causes a vapor fraction $\gamma^{in}_t(\bar{h}_{e,svt}, p_H)$ at the turbine inlet, which is lower than a required minimum

Post-print version of the article: H. Koppauer, W. Kemmetmüller, and A. Kugi, "Model predictive control of an automotive waste heat recovery system", *Control Engineering Practice*, vol. 81, pp. 28–42, 2018. DOI: 10.1016/j.conengprac.2018.09.005
The content of this post-print version is identical to the published paper but without the publisher's final layout or copy editing.

limit $\gamma_{t,min}^{in}$ (for the calculation of the specific enthalpy $\bar{h}_{e,svt}$ in the piping from the switching valve to the turbine inlet see [11]). Thus, the system has to be operated in the bypass mode to prevent droplet erosion of the turbine blades. As the reference $\bar{h}_{e,H}^{ref}$ cannot be reached in this case, the resulting large control deviation $\bar{h}_{e,H} - \bar{h}_{e,H}^{ref}$ would have a negative influence on the control performance. In order to obtain a meaningful reference for $T_{ex}^{in} \leq T_{ex,min}^{in}$, a reference $\Delta h_{sh}^{T}(T_{ex}^{in})$ is defined such that the working fluid at the inlet of the bypass switching valve is as hot as possible. This reference $\Delta h_{sh}^{T}(T_{ex}^{in})$ is calculated by maximizing the specific enthalpy $\bar{h}_{e,H}$. The overall reference for the superheating is given by

$$\Delta h_{sh}(p_H, T_{ex}^{in}) = \begin{cases} \Delta h_{sh}^{p}(p_H) & \text{for } T_{ex}^{in} \geq T_{ex,min}^{in} \\ \Delta h_{sh}^{pT}(p_H, T_{ex}^{in}) & \text{for } T_{ex}^{in} < T_{ex,min}^{in} \end{cases} \tag{25}$$

with

$$\Delta h_{sh}^{pT}(p_H, T_{ex}^{in}) = \max[\min[\Delta h_{sh}^{p}(p_H), \Delta h_{sh}^{T}(T_{ex}^{in})], \Delta h_{sh,min}] \tag{26}$$

and $\Delta h_{sh,min}$ as the minimum value of $\Delta h_{sh}^{p}(p_H)$. The resulting characteristics of $\Delta h_{sh}(p_H, T_{ex}^{in})$ is depicted in Fig. 10.

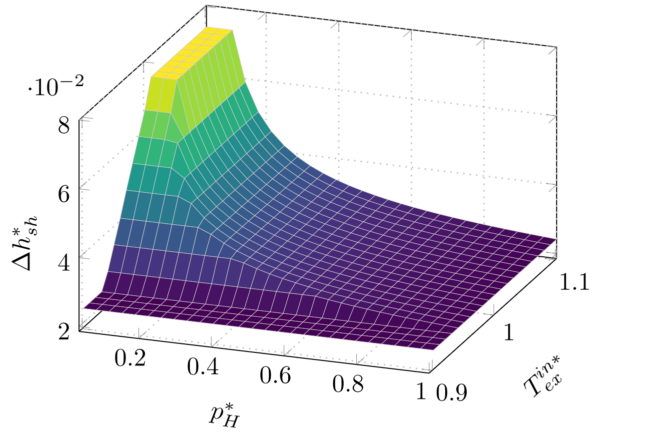

Figure 10: Normalized reference for the superheating Δh_{sh} of $\bar{h}_{e,H}$.

A second point in order to maximize the recovered energy is to prevent opening of the exhaust gas bypass valve of the evaporator in normal operation, i.e., χ_{ex} should be equal to 1 as long as this is possible, see also (4).

For a safe system operation of the WHR system, the control strategy has to ensure compliance with the following limits of the system:

(i) The working fluid decomposes at high temperatures. Thus, the temperature $T_{e,n}$ at the evaporator outlet (highest working fluid temperature in the system) is limited by

$$T_{e,n}(p_H, h_{e,n}) \leq T_{e,max}. \tag{27}$$

(ii) The construction of the system components limits the pressure p_H to

$$p_H \leq p_{H,max}. \tag{28}$$

(iii) The constraints on the control inputs $\dot{m}_p$ and χ_{ex} are expressed as[2]

$$\dot{m}_{p,min} \leq \dot{m}_p \leq \dot{m}_{p,max}, \tag{29a}$$
$$0 \leq \chi_{ex} \leq 1. \tag{29b}$$

(iv) The vapor quality (equivalent to the vapor fraction γ_t^{in}) should not fall below a certain minimum. Although the designed reference value $\bar{h}_{e,H}^{ref}$ already considers this demand, it makes sense to impose the additional constraint

$$\bar{h}_{e,H} \geq h_e''(p_H) + \Delta h_l \tag{30}$$

with $\Delta h_l \leq \Delta h_{sh}(p_H, T_{ex}^{in})$.

4.2. *Model predictive control strategy*

In this work, a model predictive control strategy is proposed to meet the control objectives formulated in the previous section. For the MPC, an optimal control problem (OCP) is designed to track the reference trajectory for $\bar{h}_{e,H}$ according to (24), (25), which is calculated with the measured quantities $p_{H,k}$ and $T_{ex,k}^{in}$ at the actual instant of time $t = k\tau_s^{ctrl}$, where τ_s^{ctrl} denotes the controller sampling time. Fig. 11 gives a qualitative illustration of the receding horizon OCP, which is defined on a prediction horizon $\tau_{ph} = n_{ph}\tau_s^{pred}$ and a control horizon $\tau_{ch} = n_{ch}\tau_s^{pred}$, characterized by the number of prediction steps n_{ph}, the number of predicted future control inputs n_{ch}, and the sampling time of the prediction model τ_s^{pred}. To keep the number of optimization variables low, the control horizon is chosen shorter than the prediction horizon and the control variables are kept constant for $t \geq k\tau_s^{ctrl} + \tau_{ch}$.

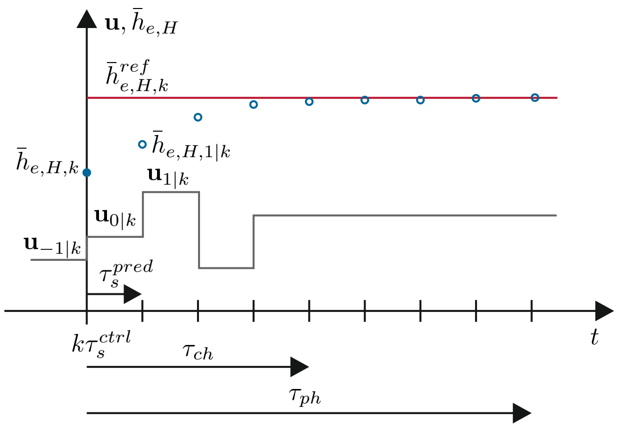

Figure 11: Qualitative illustration of the optimal control problem.

The control objectives formulated in the previous section are taken into account in the cost function J_k of the OCP in the following form

$$J_k = \left\| \bar{\mathbf{h}}_{e,H,k} - \bar{h}_{e,H,k}^{ref} \mathbf{1}_{n_{ph}\times 1} \right\|_{\mathbf{Q}}^2 + \|\delta \mathbf{U}_k\|_{\mathbf{R}_k}^2 + \beta_{ex} \left\| \mathbf{1}_{n_{ch}\times 1} - \boldsymbol{\chi}_{ex,k} \right\|^2 + \beta_{\varepsilon} \|\boldsymbol{\varepsilon}_k\|^2. \tag{31}$$

[2]The minimum pump mass flow $\dot{m}_{p,min}$ is chosen such that it prevents overheating and thus damage of the evaporator.

Post-print version of the article: H. Koppauer, W. Kemmetmüller, and A. Kugi, “Model predictive control of an automotive waste heat recovery system”, *Control Engineering Practice*, vol. 81, pp. 28–42, 2018. DOI: 10.1016/j.conengprac.2018.09.005

Therein, the vectors $\bar{\mathbf{h}}_{e,H,k}$, $\delta\mathbf{U}_k$, $\boldsymbol{\chi}_{ex,k}$, and $\boldsymbol{\varepsilon}_k$ are introduced as

$$\bar{\mathbf{h}}_{e,H,k} = [\bar{h}_{e,H,1|k}, \bar{h}_{e,H,2|k}, \cdots, \bar{h}_{e,H,n_{ph}|k}]^{\mathrm{T}}, \tag{32a}$$
$$\delta\mathbf{U}_k = [\delta\mathbf{u}_{0|k}^{\mathrm{T}}, \delta\mathbf{u}_{1|k}^{\mathrm{T}}, \cdots, \delta\mathbf{u}_{n_{ch}-1|k}^{\mathrm{T}}]^{\mathrm{T}}, \tag{32b}$$
$$\boldsymbol{\chi}_{ex,k} = [\chi_{ex,0|k}, \chi_{ex,1|k}, \cdots, \chi_{ex,n_{ch}-1|k}]^{\mathrm{T}}, \tag{32c}$$
$$\boldsymbol{\varepsilon}_k = [\varepsilon_{1|k}, \varepsilon_{2|k}, \cdots, \varepsilon_{n_{ph}|k}]^{\mathrm{T}}. \tag{32d}$$

The reference is defined according to (24), (25) by $\bar{h}_{e,H,k}^{ref} = h_e''(p_{H,k}) + \Delta h_{sh}(p_{H,k}, T_{ex,k}^{in})$ and kept constant over the prediction horizon τ_{ph}. Moreover, $\|\mathbf{x}\|_{\mathbf{Q}}^2$ denotes the weighted norm $\|\mathbf{x}\|_{\mathbf{Q}}^2 = \mathbf{x}^{\mathrm{T}}\mathbf{Q}\mathbf{x}$ with the positive definite weighting matrix $\mathbf{Q}$.

Remark 2. *In the vectors* (32a)-(32d)*, an index $i|k$ identifies the quantity at time $t = k\tau_s^{ctrl} + i\tau_s^{pred}$ based on the (measured) quantity at $t = k\tau_s^{ctrl}$. Therein τ_s^{ctrl} is the sampling time of the MPC. As it will be explained later it is meaningful to use $\tau_s^{pred} \neq \tau_s^{ctrl}$ for the prediction model.*

The first part of J_k accounts for the tracking of the desired reference $\bar{h}_{e,H,k}^{ref}$ and the third part with the scalar weighting factor $\beta_{ex} > 0$ is responsible to keep the exhaust gas bypass valve closed (i.e., $\chi_{ex} = 1$) in normal operation. To avoid fast changes in the control inputs $\mathbf{u}_{i|k}$, the incremental control inputs $\delta\mathbf{u}_{i|k} = \mathbf{u}_{i|k} - \mathbf{u}_{i-1|k}$ (with $\mathbf{u}_{-1|k} = \mathbf{u}_{0|k-1}$) are penalized in the cost function.

The incremental control inputs are weighted with

$$\mathbf{R}_k = \frac{1}{\sum_{l=1}^{n_{OP}} \zeta_l(p_{H,k})\dot{m}_{p,s,l}}\mathbf{R}_0, \tag{33}$$

where $\mathbf{R}_0$ is a constant positive definite matrix and $\dot{m}_{p,s,l}$ are the pump mass flows at the nominal operating points utilized in the gain scheduling model. The operating point dependent weighting (33) is used to account for the large changes of the control input with respect to the operating points.

The slack variables $\boldsymbol{\varepsilon}$ (scalar weighting factor β_ε) are introduced to soften the constraints (30) in the form

$$\bar{\mathbf{h}}_{e,H,k} \geq \mathbf{h}_{e,k}'' + \Delta h_l \mathbf{1}_{n_{ph}\times 1} - \boldsymbol{\varepsilon}_k \tag{34}$$

with

$$\mathbf{h}_{e,k}'' = \left[h_e''(p_{H,1|k}), h_e''(p_{H,2|k}), \cdots, h_e''(p_{H,n_{ph}|k})\right]^{\mathrm{T}}, \tag{35}$$

cf. [27]. This is necessary to avoid an infeasible OCP, which would occur for very small exhaust gas heat flow rates. The overall inequality constraints (27), (28), (29), and (34) can be summarized in the form

$$\mathbf{g}(\mathbf{U}_k, \mathbf{Y}_k, \boldsymbol{\varepsilon}_k) \leq \mathbf{0} \tag{36}$$

with the predicted control inputs $\mathbf{U}_k = [\mathbf{u}_{0|k}^{\mathrm{T}}, \mathbf{u}_{1|k}^{\mathrm{T}}, \cdots, \mathbf{u}_{n_{ch}-1|k}^{\mathrm{T}}]^{\mathrm{T}}$ and the predicted outputs $\mathbf{Y}_k = [\mathbf{y}_{1|k}^{\mathrm{T}}, \mathbf{y}_{2|k}^{\mathrm{T}}, \cdots, \mathbf{y}_{n_{ph}|k}^{\mathrm{T}}]^{\mathrm{T}}$.

The final part required to formulate the OCP is the calculation of the predicted outputs $\mathbf{y}_{i|k} = \left[h_{e,n,i|k}, p_{H,i|k}, \bar{h}_{e,H,i|k}\right]$ according to (22). For this, the exogenous inputs $\mathbf{v}_k = \left[\dot{m}_{ex,k}, T_{ex,k}^{in}, h_{p,k}^{in}, T_{amb,k}, p_{L,k}\right]^{\mathrm{T}}$ and the estimated parameters $\boldsymbol{\theta}_k = \left[\Delta\dot{Q}_{ex,k}, \Delta\dot{Q}_{H,k}\right]$ are set constant over the entire prediction horizon. This has to be done because there is no meaningful prediction of $\dot{m}_{ex}^{in}$, T_{ex}^{in} and $\boldsymbol{\theta}$ possible. Moreover, it is reasonable to assume a slow variation of T_{amb} and, as was briefly discussed in Section 3.2, the influence of the small changes in p_L and h_p^{in} in a controlled operation of the system are negligible.

Given the state $\mathbf{x}_k$ at the current instant of time $t = k\tau_s^{ctrl}$ and taking advantage of the affine structure of the dynamics (21) of the gain scheduling model, the predicted outputs $\mathbf{y}_{i|k,l}$ of the l-th local model at time $t = k\tau_s^{ctrl} + i\tau_s^{pred}$ can be written in the form

$$\mathbf{y}_{i|k,l} = \mathbf{C}\left(\mathbf{x}_{s,l} + \boldsymbol{\Phi}_l^i \Delta\mathbf{x}_{k,l} + \sum_{j=0}^{i-1} \boldsymbol{\Phi}_l^{i-j-1}\boldsymbol{\Gamma}_l \mathbf{u}_{j|k} - \sum_{j=0}^{i-1} \boldsymbol{\Phi}_l^j (\boldsymbol{\Gamma}_l \mathbf{u}_{s,l} - \mathbf{N}_{k,l})\right) \tag{37}$$

with $\Delta\mathbf{x}_{k,l} = \mathbf{x}_k - \mathbf{x}_{s,l}$ and $\boldsymbol{\Phi}_l$, $\boldsymbol{\Gamma}_l$, and $\mathbf{N}_{k,l}$ defined in Section 3.3 and evaluated for $\tau_s = \tau_s^{pred}$. Note that based on the assumptions above $\mathbf{N}_{k,l}$ is also constant over the prediction horizon.

The real-time implementation of the MPC requires an efficient solution of the OCP with the cost function (31) and the inequality constraints (36). Using (37) in the cost function (31), the cost function can be written as a quadratic function

$$J_k = J_{c,k} + \mathbf{k}_k^{\mathrm{T}}\boldsymbol{\vartheta}_k + \boldsymbol{\vartheta}_k^{\mathrm{T}}\mathbf{H}_k\boldsymbol{\vartheta}_k \tag{38}$$

with the optimization variables $\boldsymbol{\vartheta}_k = [\mathbf{U}_k^{\mathrm{T}}, \boldsymbol{\varepsilon}_k^{\mathrm{T}}]^{\mathrm{T}}$. Therein, $J_{c,k}$ is independent of $\boldsymbol{\vartheta}_k$, $\mathbf{k}_k$ accounts for the terms linear in $\boldsymbol{\vartheta}_k$, and $\mathbf{H}_k$ accounts for the quadratic terms. To yield a quadratic program (QP) for the calculation of the optimal control inputs, the constraints (36) have to be linear in $\boldsymbol{\vartheta}_k$. Therefore, first, the Taylor series expansion of the constraints (36) is considered about $(\mathbf{Y}_{k0}, \mathbf{U}_k, \boldsymbol{\varepsilon}_k)$ with $\mathbf{Y}_{k0} = [\mathbf{y}_{0|k}^{\mathrm{T}}, \mathbf{y}_{0|k}^{\mathrm{T}}, \cdots, \mathbf{y}_{0|k}^{\mathrm{T}}]^{\mathrm{T}}$, which yields

$$\mathbf{g}(\mathbf{U}_k, \mathbf{Y}_k, \boldsymbol{\varepsilon}_k) \approx \mathbf{g}(\mathbf{U}_k, \mathbf{Y}_{k0}, \boldsymbol{\varepsilon}_k) + \left.\frac{\partial\mathbf{g}}{\partial\mathbf{Y}_k}\right|_{\mathbf{U}_k, \mathbf{Y}_{k0}, \boldsymbol{\varepsilon}_k} (\mathbf{Y}_k - \mathbf{Y}_{k0}) \leq \mathbf{0}. \tag{39}$$

Next, (37) is utilized in (39), resulting in

$$\mathbf{G}_k\boldsymbol{\vartheta}_k - \mathbf{b}_k \leq \mathbf{0} \tag{40}$$

with the matrix $\mathbf{G}_k$ and the vector $\mathbf{b}_k$. The overall simplified OCP is then given in the standard form of a QP [27]

$$\min_{\boldsymbol{\vartheta}_k} J_{c,k} + \mathbf{k}_k^{\mathrm{T}}\boldsymbol{\vartheta}_k + \boldsymbol{\vartheta}_k^{\mathrm{T}}\mathbf{H}_k\boldsymbol{\vartheta}_k \tag{41a}$$
$$\text{s.t. } \mathbf{G}_k\boldsymbol{\vartheta}_k \leq \mathbf{b}_k, \tag{41b}$$

Post-print version of the article: H. Koppauer, W. Kemmetmüller, and A. Kugi, "Model predictive control of an automotive waste heat recovery system", *Control Engineering Practice*, vol. 81, pp. 28–42, 2018. DOI: 10.1016/j.conengprac.2018.09.005

which can be solved very efficiently with a state-of-the-art QP solver.

A suitable choice of the controller sampling time τ_s^{ctrl}, the prediction horizon τ_{ph}, and the control horizon τ_{ch} of the MPC is essential to obtain a high control performance and a small computational effort at the same time. A controller sampling time $\tau_s^{ctrl} = 0.4\,\mathrm{s}$ is chosen in this work, since simulation studies showed that smaller values do not increase the control performance (a similar value is used in [13]). The prediction horizon is typically chosen in a way that the main dynamic behavior of the system can be covered. As the dynamics of the system can be approximated by the plant time constant τ, it turned out that $\tau_{ph} \geq 1.5\tau$ is a good choice in this work to yield a high control performance. Furthermore, the simulation results, cf. Section 5, indicate that this choice yields a long enough prediction horizon that ensures closed-loop stability, cf. [27]. An analytical stability proof of the closed-loop system comprising the complex nonlinear model, the MPC using a gain scheduling prediction model, and the EKF seems to be impossible. Thus, the stability is analyzed based on extensive simulation studies. As demonstrated in Fig. 5, the time constant τ varies largely in the operating range, see also [22]. Thus, τ_{ph} has to be chosen as a function of p_H, i.e., $\tau_{ph}(p_H)$. Using a constant sampling time τ_s^{pred} in the prediction model would result in large changes of the number n_{ph} of the prediction steps and thus the computational effort. Instead, a constant number n_{ph} is utilized and τ_s^{pred} is adjusted to meet the currently required prediction horizon τ_{ph}. To allow for a simple transition between different values of τ_s^{pred}, it is chosen as a multiple of the minimal sampling time that is chosen equal to the controller sampling time τ_s^{ctrl}. The control horizon τ_{ch} is finally chosen to be approximately a quarter of the prediction horizon τ_{ph}.

4.3. Control of the turbine and the switching valve

The power maximizing steady-state optimization shows that the optimal rotational speed n_t of the turbine is a function of the turbine pressure ratio p_H/p_L only, i.e., $n_t(p_H/p_L)$, see [11]. Furthermore, the rotational speed of the turbine does not influence the turbine mass flow $\dot{m}_t$ and thus the control of the high-pressure part, which was discussed in the previous sections. Therefore, the generator coupled to the turbine is used to control the rotational speed of the turbine with the reference $n_t^{ref} = n_t(p_H/p_L)$. For this coupled system, it can be assumed that the turbine speed accurately tracks the desired reference, since the dynamics of the speed controlled system is considerably faster than the dynamics of the thermodynamic part of the WHR system. The design of this speed controller is not considered as a part of this contribution.

If the vapor fraction γ_t^{in} at the turbine inlet is lower than the minimum permitted vapor fraction $\gamma_{t,min}^{in}$, the system must be operated in the bypass mode (expansion over the bypass throttle) to prevent droplet erosion of the turbine. To switch between the bypass and the turbine mode, the bypass switching valve is actuated. As the working fluid state is not measured at the turbine inlet, the switching valve must be actuated based on the measurement of the specific enthalpy $\bar{h}_{e,H}$ at the inlet of the switching valve. Thus, a minimum required value $\bar{h}_{e,H,min}$ of the specific enthalpy $\bar{h}_{e,H}$ is calculated based on the steady-state system model (see [11]) that corresponds to the minimum vapor quality $\gamma_{t,min}^{in}$. If $\bar{h}_{e,H}$ is below this minimum value, the system is operated in the bypass mode. To avoid jittering of the switching valve at the switching boundary $\bar{h}_{e,H,min}$, a switching hysteresis is added.

4.4. State estimation

The proposed model predictive control strategy requires knowledge of the system states $\mathbf{x}$. In the real system, only the pressure p_H and the temperatures $T_{e,n}$ and $\bar{T}_{e,H}$ are measured. Thus, a state estimation is required. The design of the state estimation is again based on the local partially linearized models of Section 3.3. For the estimator design, the following points are considered: (i) To increase the model accuracy for operating points with very low exhaust gas inlet temperatures $T_{ex}^{in} \leq T_{ex,min}^{in}$, additional local linearized models are derived in this operating region. This results in an increased set of $n_{OP}^{kf} > n_{OP}$ local linearized models.[3] (ii) The estimator model is extended by the model for the unknown heat flow rates $\boldsymbol{\theta}$ in the form $\boldsymbol{\theta}_{k+1} = \boldsymbol{\theta}_k$. (iii) The estimation of the pressure p_H is not necessary and better estimation results can be obtained if it is considered as a known input to the model. The resulting discrete time model (sampling time τ_s^{ctrl}) for the design of the estimator reads as

$$\begin{aligned}\mathbf{x}_{k+1}^r = \sum_{l=1}^{n_{OP}^{kf}} \zeta_l(p_{H,k}) \Big(& \mathbf{x}_{s,l}^r + \mathbf{\Phi}_l^r \left(\mathbf{x}_k^r - \mathbf{x}_{s,l}^r\right) + \mathbf{\Gamma}_l^r(\mathbf{u}_k - \mathbf{u}_{s,l}) \\ & + \widetilde{\mathbf{N}}_{k,l}^r + \mathbf{\Gamma}_{\boldsymbol{\theta},l}^r \boldsymbol{\theta}_k + \mathbf{\Gamma}_{p_H,l}^r (p_{H,k} - p_{H,s,l}) \Big) + \mathbf{w}_{\mathbf{x},k}\end{aligned} \tag{42a}$$

$$\boldsymbol{\theta}_{k+1} = \boldsymbol{\theta}_k + \mathbf{w}_{\boldsymbol{\theta},k} \tag{42b}$$

$$\mathbf{y}_k^r = \mathbf{C}^r \mathbf{x}_k^r + \mathbf{v}_{\mathbf{y},k}, \tag{42c}$$

with the reduced state

$$\mathbf{x}^r = [\bar{h}_{e,1}, .., \bar{h}_{e,n}, \bar{T}_{w,1}, .., \bar{T}_{w,n}, \bar{h}_{e,H}, \bar{T}_{w,H}]^{\mathrm{T}}, \tag{43}$$

the reduced output

$$\mathbf{y}^r = [h_{e,n}, \bar{h}_{e,H}]^{\mathrm{T}}, \tag{44}$$

and

$$\widetilde{\mathbf{N}}_{k,l}^r = \int_0^{\tau_s^{ctrl}} \exp(\mathbf{A}_l^r \tau) \mathrm{d}\tau \mathbf{f}^r(\mathbf{x}_{s,l}^r, \mathbf{u}_{s,l}, \mathbf{v}_k, \mathbf{0}) \tag{45}$$

$$\mathbf{\Gamma}_{\boldsymbol{\theta},l}^r = \int_0^{\tau_s^{ctrl}} \exp(\mathbf{A}_l^r \tau) \mathrm{d}\tau \left.\frac{\partial \mathbf{f}^r}{\partial \boldsymbol{\theta}}\right|_{\mathbf{x}_{s,l}^r, \mathbf{u}_{s,l}, \mathbf{v}_{s,l}, \mathbf{0}} \tag{46}$$

$$\mathbf{\Gamma}_{p_H,l}^r = \int_0^{\tau_s^{ctrl}} \exp(\mathbf{A}_l^r \tau) \mathrm{d}\tau \left.\frac{\partial \mathbf{f}^r}{\partial p_H}\right|_{\mathbf{x}_{s,l}^r, \mathbf{u}_{s,l}, \mathbf{v}_{s,l}, \mathbf{0}}. \tag{47}$$

[3] In this operating region, the system control inputs $\dot{m}_p \approx \dot{m}_{p,min}$ and $\chi_{ex} = 1$ are near their limits and thus an improved model quality would not bring any advantage for the MPC.

Post-print version of the article: H. Koppauer, W. Kemmetmüller, and A. Kugi, "Model predictive control of an automotive waste heat recovery system", *Control Engineering Practice*, vol. 81, pp. 28–42, 2018. DOI: 10.1016/j.conengprac.2018.09.005
The content of this post-print version is identical to the published paper but without the publisher's final layout or copy editing.

Here, $\mathbf{f}^r(\mathbf{x}^r, \mathbf{u}, \mathbf{v}, \boldsymbol{\theta})$ describes the model (16) reduced by the state p_H and $\boldsymbol{\Phi}_l^r$, $\boldsymbol{\Gamma}_l^r$, $\mathbf{C}^r$, $\mathbf{A}_l^r$ are the corresponding reduced order matrices. The effect of the model uncertainties is taken into account by the bias-free Gaussian noise $\mathbf{w}_{\mathbf{x},k}$, $\mathbf{w}_{\boldsymbol{\theta},k}$, and $\mathbf{v}_{\mathbf{y},k}$, which are characterized by their covariance matrices $\mathbf{Q}_{\mathbf{x}}$, $\mathbf{Q}_{\boldsymbol{\theta}}$, and $\mathbf{R}_{\mathbf{v}}$. The entries of the diagonal matrix $\mathbf{Q}_{\mathbf{x}}$ are chosen as $4 \cdot 10^8$ for the specific enthalpies and 25 for the wall temperatures. This large difference of the entries is reasonable, since the specific enthalpies $h_e \approx 2 \cdot 10^5 - 1.3 \cdot 10^6 \mathrm{J/kg}$ and the temperatures $T_w \approx 5 \cdot 10^2\,\mathrm{K}$ differ largely in magnitude. The matrix $\mathbf{Q}_{\boldsymbol{\theta}} = \mathrm{diag}([8 \cdot 10^{-2}, 2 \cdot 10^{-2}])$ was selected to yield a fast estimation of the model-plant mismatch, but such that high-frequency oscillations of $\boldsymbol{\theta}$ are avoided. Furthermore, $\mathbf{R}_{\mathbf{v}} = \mathrm{diag}([10^9, 10^9])$ was selected to yield a good estimation quality while suppressing the influence of the sensor noise as good as possible.

The outputs $h_{e,n}$ and $\bar{h}_{e,H}$ cannot be directly measured, but are calculated from the measured pressure p_H and the measured temperatures $T_{e,n}$ and $\bar{T}_{e,H}$ using the constitutive equations of the fluid. However, this brings along the problem that the temperature of ethanol is independent of the specific enthalpy in the two-phase region, cf. (A.1) in [11]. Thus, it is not possible to calculate the specific enthalpy h_e from the measurements of p_H and T_e in this phase. To circumvent stability problems in the estimator when reaching this two-phase region of operation,[4] the following measures are taken: (i) If the two-phase region is reached, the calculated enthalpies are set to the saturation value $h_e''(p_H)$, i.e., $h_{e,n}(p_H, T_{e,n}) = h_e''(p_H)$ for $T_{e,n} \leq T_{sat}(p_H)$ and $\bar{h}_{e,H}(p_H, \bar{T}_{e,H}) = h_e''(p_H)$ for $\bar{T}_{e,H} \leq T_{sat}(p_H)$, where $T_{sat}(p_H)$ denotes the saturation (two-phase) temperature of the fluid. (ii) The estimation of $\boldsymbol{\theta}$ is stopped in this case, since otherwise a significant accumulation of errors would occur that would cause a slow convergence of the estimation when returning to the superheated vapor case. To enable a separate deactivation of this estimation, an extended Kalman filter (EKF) implementation is applied that is based on the Two-Stage Kalman Estimator described in [28]. It comprises a bias-free filter for the unbiased estimation of $\mathbf{x}_k^r$ and a bias filter for the estimation of the unknown heat flow rates $\boldsymbol{\theta}_k$. The outputs of both filters are combined to yield the estimate for the system states. The update of the estimation of $\boldsymbol{\theta}$ can be deactivated by skipping the update of the bias filter. The details of this EKF are described in Appendix A.

5. Results

The presented control concept (MPC and EKF with estimation of the heat flow rates) is tested on the validated complete nonlinear system model presented in detail in [11] for several test scenarios. The non-idealities of the sensors are taken into account by adding noise to all sensors and incorporating the dynamics of the temperature sensors. The dynamics of the working fluid pump is approximated as a PT1 element with an additional dead time.

For the controller, a prediction horizon of $n_{ch} = 40$ and a control horizon of $n_{ch} = 10$ is chosen. The parameters $\mathbf{Q} = 5.5\mathbf{I}_{n_{ph}}$ and $\mathbf{R}_0 = 10^{12}\,\mathrm{diag}([1, 10^{-3}, 1, 10^{-3}, \ldots])$ of (31), (33) were tuned based on the simulation of the closed-loop system in a defined engine reference cycle that covers a large operating range. For this, a trade-off was chosen between a good tracking performance of the desired reference $\bar{h}_{e,H}^{ref}$ and avoiding large variations of the control inputs.

Remark 3. *The large difference in magnitude of* $\mathbf{Q}$ *and* $\mathbf{R}_0$ *results from the fact that they are used for a quadratic weighting of quantities that differ largely in magnitude in the cost function* (31). *In particular, the specific enthalpy* $\bar{h}_{e,H}$ *is in the range of* $1 \cdot 10^6\,\mathrm{J/kg}$, *while the pump mass flow* $\dot{m}_p$ *is in the range of* $1 \cdot 10^{-1}\,\mathrm{kg/s}$. *If quantities normalized to* 1 *were used for* $\bar{h}_{e,H}$ *and* $\dot{m}_p$, *this would mean that the normalized tracking error of* $\bar{h}_{e,H}$ *would be weighted approximately* 50 *times higher than the variations of the normalized control input* $\dot{m}_p$.

Furthermore, the parameter $\beta_\varepsilon = 15$ was chosen large enough such that the soft constraint (34) is satisfied (at least only with small violations) as long as this is possible. For adjusting the parameter β_{ex}, the following points were taken into account: (i) To maximize the heat transfer from the exhaust gas and thus the recovered energy, the exhaust gas valve should be closed in normal system operation (i.e., $\chi_{ex} = 1$). (ii) The steady-state optimization [11] showed that, if the turbine inlet pressure p_H reaches the maximum permitted pressure $p_{H,max}$, the turbine shaft power P_t can be further increased by superheating the working fluid higher than the reference value $\bar{h}_{e,H}^{ref}$ (for the calculation of P_t see [11]). (iii) A high value of β_{ex} means that the exhaust gas valve is kept closed longer while the superheating of the working fluid increases, but then it has to be opened instantaneously if $p_H = p_{H,max}$ and $T_{e,n} = T_{e,max}$ is reached. As the exhaust gas valve could be opened too late, this could cause a violation of the maximum temperature $T_{e,max}$. Thus, $\beta_{ex} = 1.4 \cdot 10^{12}$ was selected high enough to avoid opening of the exhaust gas bypass valve in standard operation and to yield a superheating higher than the reference value $\bar{h}_{e,H}^{ref}$ for $p_H = p_{H,max}$, but low enough such that a too fast opening in the case $p_H = p_{H,max}$ and $T_{e,n} = T_{e,max}$ is avoided. The QP for the optimal control inputs (41) is solved with the MATLAB QP solver `quadprog`.

Fig. 12 displays the control performance of the presented MPC strategy with the EKF for a cold start of the WHR system in a defined engine reference cycle with the corresponding exhaust gas inlet temperature T_{ex}^{in} and exhaust gas mass flow $\dot{m}_{ex}$. The low pressure p_L and the ambient temperature T_{amb} are chosen constant during the whole simulation. After the warm-up phase, the controller tracks the reference $\bar{h}_{e,H}^{ref}$ for $\bar{h}_{e,H}$ very well. During the time periods marked with a gray background, the specific enthalpy $\bar{h}_{e,H}$ is too low to result in a sufficient vapor quality at the turbine inlet, which is mainly caused by a too low exhaust gas heat flow rate. Thus, the bypass switching valve is actuated and the working fluid expands over the bypass throttle. As a consequence, the specific enthalpy $\bar{h}_{e,svt}$ in the

[4] As already mentioned before, to protect the turbine, it has to be bypassed in this case. The system is operated near the minimum mass flow and with a fully closed exhaust gas bypass valve (i.e., $\chi_{ex} = 1$).

Post-print version of the article: H. Koppauer, W. Kemmetmüller, and A. Kugi, “Model predictive control of an automotive waste heat recovery system”, *Control Engineering Practice*, vol. 81, pp. 28–42, 2018. DOI: 10.1016/j.conengprac.2018.09.005

piping from the switching valve to the turbine inlet decreases rapidly below the saturation value $h_e''(p_H)$ (for the calculation of $\bar{h}_{e,H}$ see [11]). To meet the constraint for the maximum system pressure $p_{H,max}$, the MPC has to slightly open the exhaust gas bypass valve at $t \approx 2000\,\mathrm{s}$. The two plots at the bottom show the optimal rotational speed n_t and the resulting shaft power P_t of the turbine. The time periods with zero turbine power belong to an expansion over the bypass throttle due to an insufficient vapor quality at the turbine inlet. In conclusion, the controller can guarantee the required vapor quality at the turbine inlet during the time periods with a sufficiently high exhaust gas heat flow rate. Thus, it enables a continuous recovering of the waste heat from the exhaust gas during these periods.

To test the compensation of parameter deviations and erroneous measurements, the previous experiment is performed for changed system parameters and errors of the measured exhaust gas quantities $\dot{m}_{ex,meas}$ and $T^{in}_{ex,meas}$ defined by Scenario 3 of Tab. 1. This scenario represents the expected worst case deviations. The measurement deviation of the measured exhaust gas inlet temperature $T^{in}_{ex,meas}$ is defined as $\Delta T^{in}_{ex,meas} = T^{in}_{ex,meas} - T^{in}_{ex}$. Fig. 13 displays the simulation results. Although the MPC and the EKF are defined by the nominal system parameters, the reference $\bar{h}^{ref}_{e,H}$ can be tracked quite well. As a result, the required vapor quality at the turbine inlet can be kept almost the whole time period with a sufficiently high exhaust gas heat flow rate. The overshoots of $\bar{h}_{e,H}$ visible at certain times are due to the time the estimation of the heat flow rates needs to adapt to fast changes in the exhaust gas heat flow rate. In conclusion, this experiment shows that the proposed control concept is very robust to the investigated model-plant mismatch.

	$\frac{\alpha_{ex}}{\alpha^{nom}_{ex}}$	$\frac{\alpha_{a,H}}{\alpha^{nom}_{a,H}}$	$\frac{\dot{m}_{ex,meas}}{\dot{m}_{ex}}$	$\Delta T^{in}_{ex,meas}$
Nominal	1	1	1	0 K
Scenario 1	0.8	0.8	1	0 K
Scenario 2	0.8	0.8	0.85	-5 K
Scenario 3	1.2	1.1	1.2	5 K
Scenario 4	0.8	1.05	1.2	-5 K

Table 1: Test scenarios for deviations from the nominal parameters (superscript nom) and erroneous measurements.

To analyze the closed-loop behavior for different model-plant mismatches, the same experiment is executed for the scenarios of Tab. 1 for a system hot-start during the time period $t \in [1400, 3200]\mathrm{s}$. To demonstrate that it is meaningful to consider the unknown heat flow rates $\boldsymbol{\theta}$ for the MPC strategy, the same simulations are also performed using the nominal values $\boldsymbol{\theta} = \mathbf{0}$ for the MPC and an EKF without the estimation of the heat flow rates $\boldsymbol{\theta}$. Tab. 2 presents the results for these simulation scenarios in form of the root mean square error

$$\mathrm{RMSE} = \sqrt{\frac{1}{n_{meas}} \sum_{k=1}^{n_{meas}} \left(\bar{h}^{ref}_{e,H,k} - \bar{h}_{e,H,k}\right)^2}, \tag{48}$$

with the number of measurement samples n_{meas}, and of the time $T_{t,op}$, where the turbine operation is possible. In the nominal scenario with nominal system parameters and without measurement offsets, both MPC concepts show a similar control performance. Since the heat flow rate estimation does not improve the control performance in this case, this also indicates that the accuracy of the MPC prediction model is not significantly influenced by neglecting several effects in the control-oriented model, cf. Section 3.1, and the gain scheduling approximation. For the other scenarios, the MPC with the nominal system model has a significantly worse control performance, which results in almost zero turbine operation time for the Scenarios 3 and 4. In the Scenario 2, the MPC strategy with the nominal system model reaches $100\,\%$ turbine operation, but with a too high superheating for $\bar{h}_{e,H}$. Consequently, the system is not operated optimally and more energy could be recovered, if the optimal reference were tracked. The proposed MPC/EKF with the heat flow rate estimation can compensate for the parameter and measurement deviations for all scenarios and shows a control performance almost identical to the nominal case.

	Nominal model		HFRE	
	RMSE in kJ/kg	$T_{t,op}$ in %	RMSE in kJ/kg	$T_{t,op}$ in %
Nominal	4.9	99.7	5.0	100
Scenario 1	12.2	91.3	3.7	100
Scenario 2	26.2	100	4.9	100
Scenario 3	32.6	12.9	6.9	100
Scenario 4	41.3	5.9	8.7	99.4

Table 2: Control performance for parameter variations and erroneous measurements using the MPC strategy for the nominal system model and the proposed MPC/EKF with heat flow rate estimation (HFRE).

Fig. 14 depicts the simulation results for the system operation from low to very high engine load. In this scenario, the exhaust gas mass flow $\dot{m}_{ex}$ shows a very fast change, while the thermal inertia of the engine and the exhaust system causes a slower change of the exhaust gas inlet temperature T^{in}_{ex}. At the beginning of the simulation, the MPC tracks the reference for $\bar{h}_{e,H}$ quite well. At $t \approx 150\,\mathrm{s}$, p_H reaches its limit $p_{H,max}$. To prevent damage of the system, the MPC opens the exhaust gas bypass valve χ_{ex}. Looking at $\bar{h}_{e,H}$, $\bar{h}_{e,svt}$, and $T_{e,n}$, it is obvious that these values rise and $\bar{h}_{e,H}$ deviates from its reference value $\bar{h}^{ref}_{e,H}$. This is meaningful, since this brings along that more heat is recovered from the exhaust gas, which also leads to a slight increase of the turbine shaft power P_t. After the sudden reduction of the exhaust gas heat flow rate at $t = 300\,\mathrm{s}$, a very fast and excellent change back to the optimal reference tracking can be observed. In combination with the previous results, which also covered very small engine loads, it is shown that the proposed control concept (MPC+EKF) exhibits a high control performance in the entire operating range of the WHR system.

The computation of the overall control concept (MPC+EKF) requires an average computing time of $60\,\mathrm{ms}$ on a state-of-the-art computing hardware (Intel Core i7, $4\,\mathrm{GHz}$), where the so-

Post-print version of the article: H. Koppauer, W. Kemmetmüller, and A. Kugi, "Model predictive control of an automotive waste heat recovery system", *Control Engineering Practice*, vol. 81, pp. 28–42, 2018. DOI: 10.1016/j.conengprac.2018.09.005

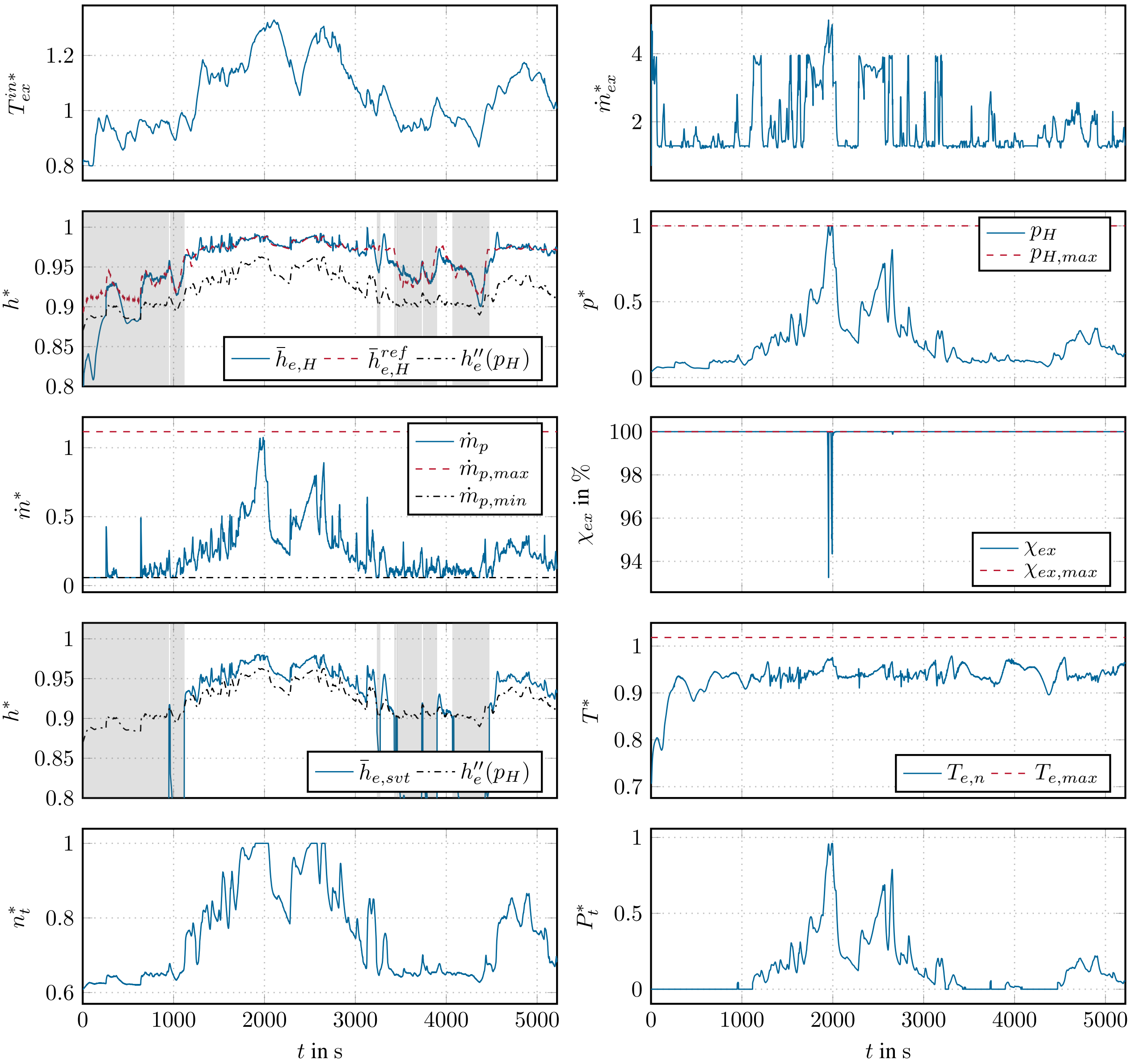

Figure 12: Closed-loop control performance for a given cold-start reference cycle - the time periods with a gray background indicate an expansion over the bypass throttle.

lution of the QP (41) takes approximately 50 ms. This is well below the controller sampling time $\tau_s^{ctrl} = 400$ ms. It has to be noted that the parameters of the QP (41) have to be calculated at every instant of time $t = k\tau_s^{ctrl}$, which takes a significant computing time of ≈ 10 ms. Thus, it is reasonable to use the reduced order model (8) instead of the full order model with 65 states for this calculation. It should be mentioned that the focus of this work is on the design of the proposed control concept but not on the optimization of the computational effort. However, if a further reduction of the computational effort is required (e.g. for implementing the control strategy on a less powerful ECU), using a QP solver tailored to the exact structure of the problem instead of the standard MATLAB solver should significantly increase the calculation speed of the MPC, see, e.g., tools like `cvxgen` [29].

6. Conclusions

This paper presented an MPC strategy for the evaporator of an automotive ORC WHR system with a radial turbine. To maximize the recovered energy from the waste heat, the proposed MPC was designed to track an optimal reference for the system states that was derived from a steady-state optimization. The MPC uses a prediction model based on a gain scheduling of local partially linearized system models. This finally yields a quadratic program for calculating the optimal control

Post-print version of the article: H. Koppauer, W. Kemmetmüller, and A. Kugi, "Model predictive control of an automotive waste heat recovery system", *Control Engineering Practice*, vol. 81, pp. 28–42, 2018. DOI: 10.1016/j.conengprac.2018.09.005
The content of this post-print version is identical to the published paper but without the publisher's final layout or copy editing.

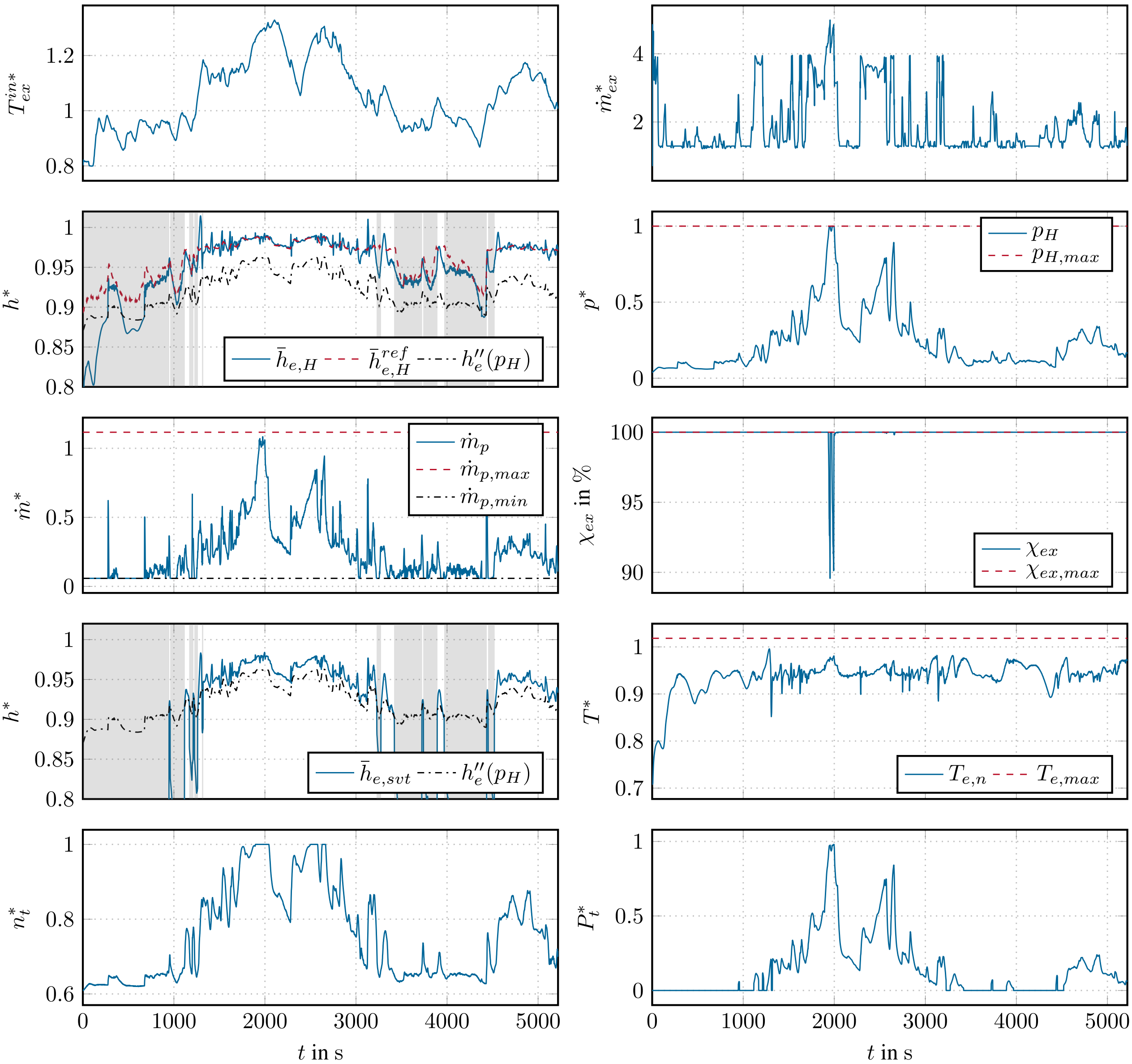

Figure 13: Closed-loop control performance for a given cold-start reference cycle with parameter deviations and erroneous measurements - the time periods with a gray background indicate an expansion over the bypass throttle.

inputs, which can be efficiently solved by a state-of-the-art QP solver. Furthermore, the control strategy comprises an extended Kalman filter with an estimation of the model-plant mismatches to guarantee a robust system control.

The developed control concept shows a good tracking performance of the optimal reference in the entire operating range of the WHR system and thus enables the optimal recovering of the exhaust gas heat. This was proven on a validated, highly accurate simulation model for a defined engine reference cycle. In the practical application, erroneous measurements of the exhaust gas quantities and non-negligible changes of the system parameters are expected. As it was shown in the simulation, an MPC concept that does not consider this model-plant mismatch yields large deviations from the desired optimal reference, which can even lead to a recovered energy equal to zero. The simulation of the proposed MPC combined with an estimator of the model-plant mismatch shows that this control concept succeeds in tracking the desired optimal reference. To discuss further possible benefits of the proposed control concept, it is compared to selected state-of-the-art control concepts for WHR systems:[5]

(i) In [3], the controller combines a nonlinear feedforward

[5] As the system configurations and the investigated experiments are not identical, the results cannot be compared directly. Thus, the comparison is based on rating the features of each control concept and the corresponding simulation and measurement results.

Post-print version of the article: H. Koppauer, W. Kemmetmüller, and A. Kugi, "Model predictive control of an automotive waste heat recovery system", *Control Engineering Practice*, vol. 81, pp. 28–42, 2018. DOI: 10.1016/j.conengprac.2018.09.005
The content of this post-print version is identical to the published paper but without the publisher's final layout or copy editing.

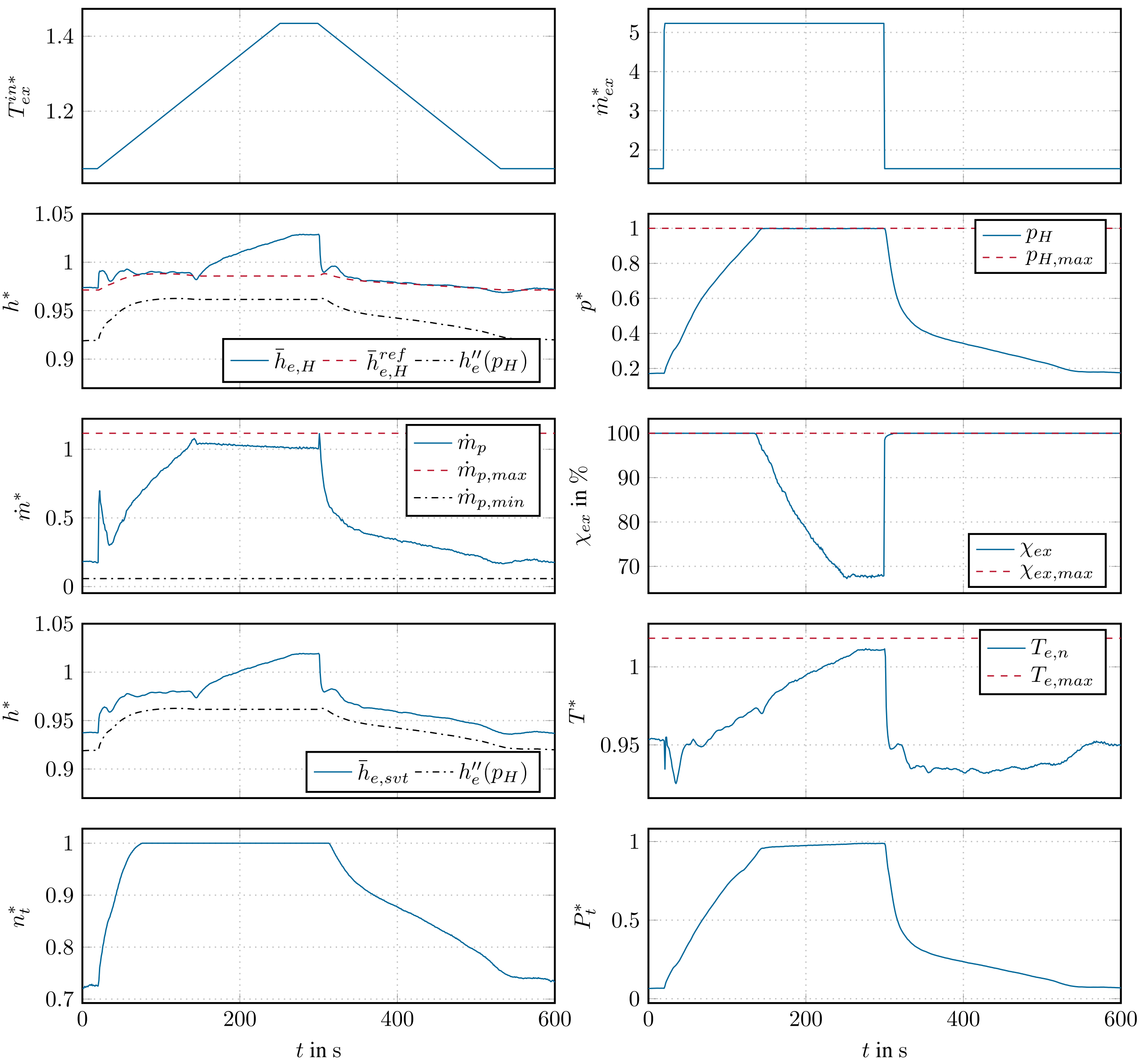

Figure 14: Closed loop control performance for the system operation from low to very high engine load.

with a feedback control using a gain scheduling of 5 LQR controllers. As the LQR controllers are based on reduced order models with 3 states, the calculation of the feedforward and the feedback control requires little computational effort and thus this concept is suitable for a real-time implementation. However, this control concept cannot handle constraints of the system states and thus it may not guarantee a safe system operation. Furthermore, the simulation and measurement results show rather large fluctuations of the temperature at the inlet of the expansion machine and the authors indicate that, therefore, the use of a turbine is not advisable. This concept uses an estimation of selected heat transfer coefficients that are used in the feedforward control. However, the influence of parameter deviations on the closed-loop control performance was not examined in this article.

(ii) To handle input constraints and state constraints at the expander inlet, the authors of [13] present a linear MPC for a dual evaporator WHR system that switches the reduced order prediction and state estimator models based on the actual exhaust gas heat flow rate. This linear MPC also requires the solution of a QP. Thus, it can be expected that the time to calculate the optimal control inputs is similar to the time to solve the QP (41). The drawbacks of this MPC concept are that it cannot compensate for a large model-plant mismatch and the switching can

Post-print version of the article: H. Koppauer, W. Kemmetmüller, and A. Kugi, "Model predictive control of an automotive waste heat recovery system", *Control Engineering Practice*, vol. 81, pp. 28–42, 2018. DOI: 10.1016/j.conengprac.2018.09.005
The content of this post-print version is identical to the published paper but without the publisher's final layout or copy editing.

produce bumps of the estimated states, since the reduced order models do not preserve the same system states. As a consequence, the variations of the control inputs had to be penalized to avoid aggressive plant actuation, see [13]. Furthermore, the presented simulation results show rather large deviations of the controlled variable (the evaporator outlet vapor fraction) from the desired reference. Thus, it can be expected that the control concept of the present work has a superior control performance, which can be attributed to systematically considering the nonlinear influence of the exogenous inputs in the local models (21) and the smooth transition between the local models in the prediction model (22).

(iii) The authors of [13] also examined nonlinear MPC for WHR systems in simulations, see also [17]. The presented simulation results show that the nonlinear MPC has a control performance which is superior to the linear MPC, but it is not real-time capable using a sampling time of $400\,\mathrm{ms}$, see [13]. In comparison, the proposed control concept of the present work approximately considers several system nonlinearities, like the nonlinear influence of the exogenous inputs and the operating point dependent system dynamics. Although the computational effort is higher compared to a standard linear MPC, it is significantly lower than for a nonlinear MPC (computing time $t > 400\,\mathrm{ms}$, cf. [13]). With a computing time of $60\,\mathrm{ms}$, the control concept proposed in this paper can be implemented on a state-of-the-art ECU.

(iv) In contrast to several state-of-the-art concepts, the proposed control concept tracks an optimal reference that was derived from the results of a steady-state optimization and considers the heat losses to the turbine inlet. This maximizes the recovered energy, while guaranteeing the minimum required vapor quality at the turbine inlet.

In conclusion, the presented control concept satisfies the control objective of the high-pressure part of the considered WHR system. The optimal dynamic system operation further requires a suitable control of the turbine outlet pressure p_L to maximize the turbine shaft power. Thus, current work is concerned with an MPC strategy for the low-pressure part of the WHR system and subsequently with the optimal control of the whole system to maximize the recovered energy.

Acknowledgements

The authors thank Robert Bosch GmbH for funding this project. In particular, the authors highly appreciate the support of Carolina Passenberg, Derya Lindenmeier, and Matthias Bitzer.

Appendix A. Two-Stage Kalman Estimator

In this appendix, the equations of the Two-Stage Kalman Estimator for the system are summarized. Details on the theoretic foundation are presented in [28].

The bias-free filter for the system (42)-(45) consists of the prediction step for the (unbiased) reduced system states $\bar{\mathbf{x}}_k^r$ and the covariance $\mathbf{P}_{\bar{\mathbf{x}}^r,k}$

$$\begin{aligned}\bar{\mathbf{x}}_k^{r-} &= \sum_{l=1}^{n_{OP}^{kf}} \zeta_l(p_{H,k-1})\big(\mathbf{x}_{s,l}^r + \boldsymbol{\Phi}_l^r\big(\bar{\mathbf{x}}_{k-1}^{r+} - \mathbf{x}_{s,l}^r\big)\\ &\quad + \boldsymbol{\Gamma}_l^r(\mathbf{u}_{k-1} - \mathbf{u}_{s,l}) + \tilde{\mathbf{N}}_{k-1,l}^r\\ &\quad + \boldsymbol{\Gamma}_{p_H,l}^r(p_{H,k-1} - p_{H,s,l})\big) + \boldsymbol{\kappa}_{k-1} \qquad \text{(A.1a)}\\ \mathbf{P}_{\bar{\mathbf{x}}^r,k}^- &= \sum_{l=1}^{n_{OP}^{kf}} \zeta_l(p_{H,k-1})\Big(\boldsymbol{\Phi}_l^r \mathbf{P}_{\bar{\mathbf{x}}^r,k-1}^+ \boldsymbol{\Phi}_l^{r\mathrm{T}}\Big) + \bar{\mathbf{Q}}_{k-1} \qquad \text{(A.1b)}\end{aligned}$$

and the update step using the measurements $\mathbf{y}_k^r$

$$\begin{aligned}\hat{\mathbf{L}}_{\bar{\mathbf{x}}^r,k} &= \mathbf{P}_{\bar{\mathbf{x}}^r,k}^- \mathbf{C}^{r\mathrm{T}}\Big(\mathbf{C}^r \mathbf{P}_{\bar{\mathbf{x}}^r,k}^- \mathbf{C}^{r\mathrm{T}} + \mathbf{R}_{\mathbf{v}}\Big)^{-1} \qquad \text{(A.2a)}\\ \bar{\mathbf{x}}_k^{r+} &= \bar{\mathbf{x}}_k^{r-} + \hat{\mathbf{L}}_{\bar{\mathbf{x}}^r,k}\big(\mathbf{y}_k^r - \mathbf{C}^r \bar{\mathbf{x}}_k^{r-}\big) \qquad \text{(A.2b)}\\ \mathbf{P}_{\bar{\mathbf{x}}^r,k}^+ &= \Big(\mathbf{I} - \hat{\mathbf{L}}_{\bar{\mathbf{x}}^r,k}\mathbf{C}^r\Big)\mathbf{P}_{\bar{\mathbf{x}}^r,k}^-. \qquad \text{(A.2c)}\end{aligned}$$

The quantities utilized in (A.1) read as

$$\begin{aligned}\boldsymbol{\kappa}_{k-1} &= \big(\bar{\mathbf{W}}_k - \mathbf{W}_k\big)\hat{\boldsymbol{\theta}}_{k-1}^+ \qquad \text{(A.3a)}\\ \bar{\mathbf{W}}_k &= \sum_{l=1}^{n_{OP}^{kf}} \zeta_l(p_{H,k-1})\big(\boldsymbol{\Phi}_l^r \mathbf{V}_{k-1} + \boldsymbol{\Gamma}_{\boldsymbol{\theta},l}^r\big) \qquad \text{(A.3b)}\\ \mathbf{W}_k &= \bar{\mathbf{W}}_k\bigg(\mathbf{I} - \mathbf{Q}_{\boldsymbol{\theta}}\Big(\mathbf{P}_{\boldsymbol{\theta},k}^-\Big)^{-1}\bigg) \qquad \text{(A.3c)}\\ \mathbf{V}_k &= \mathbf{W}_k - \hat{\mathbf{L}}_{\bar{\mathbf{x}}^r,k}\mathbf{S}_k \qquad \text{(A.3d)}\\ \mathbf{S}_k &= \mathbf{C}^r \mathbf{W}_k \qquad \text{(A.3e)}\\ \bar{\mathbf{Q}}_{k-1} &= \mathbf{Q}_{\mathbf{x}} + \mathbf{W}_k\big(\bar{\mathbf{W}}_k \mathbf{Q}_{\boldsymbol{\theta}}\big)^{\mathrm{T}}. \qquad \text{(A.3f)}\end{aligned}$$

Analogously, the bias filter for the unknown heat flow rates $\hat{\boldsymbol{\theta}}_k$ with the covariance $\mathbf{P}_{\hat{\boldsymbol{\theta}},k}$ is given by

$$\begin{aligned}\hat{\boldsymbol{\theta}}_k^- &= \hat{\boldsymbol{\theta}}_{k-1}^+ \qquad \text{(A.4a)}\\ \mathbf{P}_{\hat{\boldsymbol{\theta}},k}^- &= \mathbf{P}_{\hat{\boldsymbol{\theta}},k-1}^+ + \mathbf{Q}_{\boldsymbol{\theta}} \qquad \text{(A.4b)}\end{aligned}$$

and

$$\begin{aligned}\hat{\mathbf{L}}_{\hat{\boldsymbol{\theta}},k} &= \mathbf{P}_{\hat{\boldsymbol{\theta}},k}^- \mathbf{S}_k^{\mathrm{T}}\Big(\mathbf{C}^r \mathbf{P}_{\bar{\mathbf{x}}^r,k}^- \mathbf{C}^{r\mathrm{T}} + \mathbf{R}_{\mathbf{v}} + \mathbf{S}_k \mathbf{P}_{\hat{\boldsymbol{\theta}},k}^- \mathbf{S}_k^{\mathrm{T}}\Big)^{-1} \qquad \text{(A.5a)}\\ \hat{\boldsymbol{\theta}}_k^+ &= \hat{\boldsymbol{\theta}}_k^- + \hat{\mathbf{L}}_{\hat{\boldsymbol{\theta}},k}\Big(\mathbf{y}_k^r - \mathbf{C}^r \bar{\mathbf{x}}_k^{r-} - \mathbf{S}_k \hat{\boldsymbol{\theta}}_k^-\Big) \qquad \text{(A.5b)}\\ \mathbf{P}_{\hat{\boldsymbol{\theta}},k}^+ &= \Big(\mathbf{I} - \hat{\mathbf{L}}_{\hat{\boldsymbol{\theta}},k}\mathbf{S}_k\Big)\mathbf{P}_{\hat{\boldsymbol{\theta}},k}^-. \qquad \text{(A.5c)}\end{aligned}$$

Combining the estimates of the two filters gives the estimate $\hat{\mathbf{x}}_k^r$ for the reduced state vector $\mathbf{x}^r$ and the corresponding covariance $\mathbf{P}_{\hat{\mathbf{x}}^r,k}$

$$\begin{aligned}\hat{\mathbf{x}}_k^{r+} &= \bar{\mathbf{x}}_k^{r+} + \mathbf{V}_k \hat{\boldsymbol{\theta}}_k^+ \qquad \text{(A.6a)}\\ \mathbf{P}_{\hat{\mathbf{x}}^r,k}^+ &= \mathbf{P}_{\bar{\mathbf{x}}^r,k}^+ + \mathbf{V}_k \mathbf{P}_{\hat{\boldsymbol{\theta}},k}^+ \mathbf{V}_k^{\mathrm{T}}. \qquad \text{(A.6b)}\end{aligned}$$

To deactivate the estimation of the unknown heat flow rates $\boldsymbol{\theta}$, the update step (A.5) is skipped and (A.4) is changed to

$$\hat{\boldsymbol{\theta}}_k^+ = \hat{\boldsymbol{\theta}}_{k-1}^+ \qquad \text{(A.7)}$$

$$\mathbf{P}_{\hat{\boldsymbol{\theta}},k}^+ = \mathbf{P}_{\hat{\boldsymbol{\theta}},k-1}^+. \qquad \text{(A.8)}$$

Post-print version of the article: H. Koppauer, W. Kemmetmüller, and A. Kugi, “Model predictive control of an automotive waste heat recovery system”, *Control Engineering Practice*, vol. 81, pp. 28–42, 2018. doi: 10.1016/j.conengprac.2018.09.005
The content of this post-print version is identical to the published paper but without the publisher’s final layout or copy editing.

References

References

[1] L. Arnaud, G. Ludovic, D. Mouad, Z. Hamid, L. Vincent, Comparison and Impact of Waste Heat Recovery Technologies on Passenger Car Fuel Consumption in a Normalized Driving Cycle, Energies 7 (2014) 5273–5290.

[2] P. Tona, J. Peralez, Control of Organic Rankine Cycle Systems on board Heavy-Duty Vehicles: a Survey, IFAC-PapersOnLine 48 (15) (2015) 419–426.

[3] D. Seitz, O. Gehring, C. Bunz, M. Brunschier, O. Sawodny, Design of a Nonlinear, Dynamic Feedforward Part for the Evaporator Control of an Organic Rankine Cycle in Heavy Duty vehicles, IFAC-PapersOnLine 49 (11) (2016) 625–632.

[4] D. Luong, T.-C. Tsao, Linear Quadractic Integral Control of an Organic Rankine Cycle for Waste Heat Recovery in Heavy-Duty Diesel Powertrain, in: Proceedings of the American Control Conference, Portland, 2014, pp. 3147–3152.

[5] J. Peralez, P. Tona, A. Sciarretta, P. Dufour, M. Nadri, Towards model-based control of a steam Rankine process for engine waste heat recovery, in: Proceedings of the IEEE Vehicle Power and Propulsion Conference, Seoul, 2012, pp. 289–294.

[6] T. A. Horst, H.-S. Rottengruber, M. Seifert, J. Ringler, Dynamic heat exchanger model for performance prediction and control system design of automotive waste heat recovery systems, Applied Energy 105 (2013) 293–303.

[7] U. Drescher, D. Brüggemann, Fluid selection for the Organic Rankine Cycle (ORC) in biomass power and heat plants, Applied Thermal Engineering 27 (2007) 223–228.

[8] J. Song, C. Gu, Performance analysis of a dual-loop organic Rankine cycle (ORC) system with wet steam expansion for engine waste heat recovery, Applied Energy 156 (2015) 280–289.

[9] S. Glover, R. Douglas, M. D. Rosa, X. Zhang, L. Glover, Simulation of a multiple heat source supercritical ORC (Organic Rankine Cycle) for vehicle waste heat recovery, Energy 93 (2015) 1568–1580.

[10] V. Grelet, T. Reiche, V. Lemort, M. Nadri, P. Dufour, Transient performance evaluation of waste heat recovery rankine cycle based system for heavy duty trucks, Applied Energy 165 (2016) 878–892.

[11] H. Koppauer, W. Kemmetmüller, A. Kugi, Modeling and optimal steady-state operating points of an ORC waste heat recovery system for diesel engines, Applied Energy 206 (2017) 329–345.

[12] M. C. Esposito, N. Pompini, A. Gambarotta, V. Chandrasekaran, J. Zhou, M. Canova, Nonlinear Model Predictive Control of an Organic Rankine Cycle for Exhaust Waste Heat Recovery in Automotive Engines, IFAC-PapersOnLine 48 (15) (2015) 411–418.

[13] E. Feru, F. Willems, B. de Jager, M. Steinbuch, Modeling and Control of a Parallel Waste Heat Recovery System for Euro-VI Heavy-Duty Diesel Engines, Energies 7 (2014) 6571–6592.

[14] D. Seitz, O. Gehring, C. Bunz, M. Brunschier, O. Sawodny, Dynamic Model of a Multi-Evaporator Organic Rankine Cycle for Exhaust Heat Recovery in Automotive Applications, in: Proceedings of the IFAC Symposium on Mechatronic Systems, Loughborough, 2016, pp. 39–46.

[15] J. Peralez, P. Tona, O. Lepreux, A. Sciaretta, L. Voise, P. Dufour, M. Nadri, Improving the Control Performance of an Organic Rankine Cycle System for Waste Heat Recovery from a Heavy-Duty Diesel Engine using a Model-Based Approach, in: Proceedings of the Conference on Decision and Control, Florence, 2013, pp. 6830–6836.

[16] D. Seitz, O. Gehring, C. Bunz, M. Brunschier, O. Sawodny, Model-based control of exhaust heat recovery in a heavy-duty vehicle, Control Engineering Practice 70 (2018) 15–28.

[17] P. Petr, C. Schröder, J. Köhler, M. Gräber, Optimal control of waste heat recovery systems applying nonlinear model predictive control (NMPC), in: Proceedings of the International Seminar on ORC Power Systems, Brussels, 2015.

[18] A. Hernandez, A. Desideri, S. Gusev, C. M. Ionescu, M. Van Den Broek, S. Quoilin, V. Lemort, R. De Keyser, Design and experimental validation of an adaptive control law to maximize the power generation of a small-scale waste heat recovery system, Applied Energy 203 (549-559).

[19] J. B. Rawlings, D. Q. Mayne, Model Predictive Control, 1st Edition, Nob Hill Publishing, Madison, 2009.

[20] L. Wang, Model Predictive Control System Design and Implementation Using MATLAB, Springer, 2009.

[21] E. Feru, B. de Jager, F. Willems, M. Steinbuch, Two-phase plate-fin heat exchanger modeling for waste heat recovery systems in diesel engines, Applied Energy 133 (2014) 183–196.

[22] E. Feru, F. Willems, G. Rascanu, C. Rojer, B. de Jager, M. Steinbuch, Control of automotive waste heat recovery systems with parallel evaporators, in: Proceedings of the FISITA World Automotive Congress 2014, 2014.

[23] J. S. Shamma, M. Athans, Analysis of Gain Scheduled Control for Nonlinear Plants, IEEE Transactions on Automatic Control 35 (1990) 898–907.

[24] K. J. Hunt, T. A. Johansen, Design and analysis of gain-scheduled control using local controller networks, International Journal of Control 66 (1997) 619–651.

[25] D. A. Lawrence, W. J. Rugh, Gain Scheduling Dynamic Linear Control for a Nonlinear Plant, Automatica 31 (1995) 381–390.

[26] D. J. Leith, W. E. Leithead, Survey of gain-scheduling analysis and design, International Journal of Control 73 (2000) 1001–1025.

[27] J. M. Maciejowski, Predictive Control with Constraints, 1^{st} Edition, Pearson Prentice Hall, 2002.

[28] C.-S. Hsieh, F.-C. Chen, Optimal Solution of the Two-Stage Kalman Estimator, IEEE Transactions on Automatic Control 44 (1999) 194–199.

[29] J. Mattingley, S. Boyd, Cvxgen: A code generator for embedded convex optimization, Optimization and Engineering 13 (2012) 1–27.

Post-print version of the article: H. Koppauer, W. Kemmetmüller, and A. Kugi, "Model predictive control of an automotive waste heat recovery system", *Control Engineering Practice*, vol. 81, pp. 28–42, 2018. DOI: 10.1016/j.conengprac.2018.09.005